



JOHANNES KEPLER UNIVERSITY OF LINZ
PHYSICAL CHEMISTRY

Photoinduced Fourier Transform Infrared (FT-IR) spectroscopy on Conjugated Polymer Films and Blends

Diploma thesis
by
Henrik Johansson

under the supervision of
Univ.-Prof. Mag. Dr. N. Serdar Sariciftci
Linz, Austria, in September 1998

Eidesstattliche Erklärung

Hiermit erkläre ich an Eides statt, die Vorliegende Diplomarbeit selbständig verfaßt, keine als die angegebenen Quellen und Hilfsmittel benutzt und mich auch sonst keiner unerlaubten Hilfe bedient zu haben.

Diese Diplomarbeit wurde bisher weder im Inland noch im Ausland als Prüfungsarbeit vorgelegt.

Linz, Österreich, September 1998

Henrik Johansson

Abstract

This work consists of an investigation on photophysical properties of thin films containing the conjugated polymers poly(3-octylthiophene) and poly(3,4-dihexyloxythiophene) in different combinations with the addition of the soluble fullerene derivative [6,6]PC₆₁BM. We investigated these solid state films by chemical, electrochemical and photoinduced doping methods. Further, we incorporated these photoinduced charge transfer systems into stable conventional host polymers such as polystyrene, polyvinylcarbazole, polycarbonate and polyvinylbenzylchloride and observed the influence of these hosts on the embedded photoactive guest. Main experimental technique has been Fourier transform infrared FT-IR spectroscopy where the absorption spectra principally are discussed with respect to the ultrafast photoinduced electron transfer from conjugated polymers onto fullerene.

Contents

LIST OF FIGURES	6
LIST OF TABLES	8
1 MOTIVATION	9
1.1 OBJECTIVE OF THESIS	9
2 INTRODUCTION	11
2.1 OVERVIEW OF ORGANIC SOLAR CELLS	11
2.1.1 <i>Operational description of the plastic solar cell</i>	11
2.2 POLYMERS HOSTS	13
2.3 POLYMER SOLUTIONS	14
2.4 CONJUGATED POLYMERS	15
3 QUASI-PARTICLES AND ELECTRON TRANSFER	17
3.1 MOLECULAR STRUCTURE	17
3.2 OPTICAL AND ELECTRONIC PROPERTIES.....	19
3.3 CHARACTERISATION OF EXCITED STATES	20
3.4 PHOTOINDUCED ELECTRON TRANSFER.....	23
3.4.1 <i>Donors and acceptors</i>	25
4 PHOTOPHYSICS AND INFRARED ACTIVITY	29
4.1 LIFE OF PHOTOEXCITED STATES	29
4.1.1 <i>Absorption</i>	29
4.1.2 <i>Relaxation</i>	30
4.2 INFRARED ACTIVATED VIBRATIONAL (IRAV) MODES.....	32
5 EXPERIMENTAL	35
5.1 FT-IR SET-UP	35
5.2 SAMPLE PREPARATION.....	36
5.3 MEASUREMENT MODES	36
5.3.1 <i>Photoinduced absorption</i>	36
5.3.2 <i>Chemically doping induced absorption</i>	37
5.3.3 <i>Electrochemically doping induced absorption</i>	37
5.4 IMPROVEMENTS OF THE MEASUREMENT SYSTEM.....	37
5.5 QUALITATIVE TO QUANTITATIVE VALUES.....	38
6 RESULTS AND DISCUSSIONS	41

6.1	COMPARATIVE DOPING STUDIES	41
6.1.1	<i>P3OT</i>	41
6.1.2	<i>PDHT</i>	45
6.2	PHOTOINDUCED ABSORPTION FOR DONOR/ACCEPTOR NETWORKS	48
6.3	INFLUENCE OF HOST MATRICES.....	52
6.3.1	<i>Low energy range</i>	53
6.3.2	<i>Higher energy range</i>	54
6.4	MORPHOLOGY	57
6.5	CONCLUSIONS	60
6.6	ACKNOWLEDGEMENTS	60
7	BIBLIOGRAPHY	63
8	APPENDIX	67
8.1	SPECIFICATIONS OF USED EQUIPMENT.....	67
8.2	ABOUT THIS WORK	67
8.3	PUBLICATIONS.....	68

List of Figures

<i>Figure 1: Comparison between a bilayer structure (left) and a bulk heterojunction structure (right) solar cell device.</i>	12
<i>Figure 2: Main operational orders of an organic solar cell with an interpenetrating network structure.</i>	13
<i>Figure 3: Host polymers for the embedding of photoactive guest materials.</i>	14
<i>Figure 4: Names and chemical structures of common conjugated polymers.</i>	16
<i>Figure 5: Structure of two equivalent trans-polyacetylene chains.</i>	17
<i>Figure 6: Polyacetylene chain before dimerisation (above) and after, (below). Modified picture from ref. [9].</i>	18
<i>Figure 7: Transition from a metallic behaviour with half-filled π-band to a bandgap semiconductor due to Peierls distortion.</i>	18
<i>Figure 8: $\pi \rightarrow \pi^*$ transition in ethene. Picture from ref. [11].</i>	19
<i>Figure 9: Neutral soliton in trans-polyacetylene.</i>	20
<i>Figure 10: Three types of solitons. Note the reversed spin-charge relation.</i>	20
<i>Figure 11: Lowest ground state energy is that of the aromatic form of polythiophene.</i>	21
<i>Figure 12: Structure, spin configuration and optical transitions for the positive and negative polarons.</i>	22
<i>Figure 13: Energy diagram of the singlet and triplet excitons.</i>	22
<i>Figure 14: Structure, spin configuration and optical transitions for the positive and negative bipolarons.</i>	23
<i>Figure 15: Schematic energy diagram for the ultrafast photoinduced electron transfer between a conjugated polymer and the buckminsterfullerene C_{60}.</i>	25
<i>Figure 16: Two types of polythiophene derivatives used as donors in the work. Left the chemical structure of P3OT and right that of PDHT.</i>	26
<i>Figure 17: Left the symmetric structure of the buckminsterfullerene (C_{60}) and right the modified and functionalised derivative [6,6]PC₆₁BM.</i>	26
<i>Figure 18: In the picture we see the mirror symmetry of the absorption spectrum (full line) and the emission spectrum (dashed line). Picture from ref. [23].</i>	29
<i>Figure 19: Electronic transitions according to the Franck-Condon principle. Picture from ref. [23].</i>	30
<i>Figure 20: Electronic excitation followed by fluorescent relaxation. Picture from ref. [23].</i>	31
<i>Figure 21: Jablonski diagram of intramolecular relaxation channels. Picture from ref. [23].</i>	32
<i>Figure 22: Plot of relative electric response χ versus energy, from ref. [32].</i>	33
<i>Figure 23: FT-IR set-up.</i>	35
<i>Figure 24: Excitation of cast pellet sample and the detection of transmitted infrared probe light.</i>	36
<i>Figure 25: Comparison of IR spectra of P3OT for different doping techniques and levels.</i>	42
<i>Figure 26: Comparison of doping induced absorption for P3OT over an extended energy range.</i>	45
<i>Figure 27: Comparison of IR spectra of PDHT for different doping techniques.</i>	46
<i>Figure 28: Comparison of doping induced absorption for PDHT over an extended energy range (smoothed spectra).</i>	48

<i>Figure 29: IR electronic absorption for P3OT with and without acceptor molecules within the network structure.</i>	49
<i>Figure 30: Enlarged low IR range for comparison of IRAV band positions for P3OT with and without PCBM.</i>	50
<i>Figure 31: IR electronic absorption for PDHT with and without acceptor molecules within the network structure.</i>	51
<i>Figure 32: Enlarged low IR range for comparison of IRAV band positions for PDHT with and without PCBM.</i>	52
<i>Figure 33: Host polymer influence on IRAV modes for P3OT.</i>	53
<i>Figure 34: Host polymer influence on IRAV modes for PDHT.</i>	54
<i>Figure 35: Weakening of photoinduced absorption for embedded P3OT/PCBM charge transfer network.</i>	55
<i>Figure 36: Photoinduced absorption for embedded PDHT/PCBM donor-acceptor networks.</i>	56
<i>Figure 37: Absorption spectra for undoped PDHT/PCBM network with and without addition of PC host.</i>	57
<i>Figure 38: Improved morphology for PCBM derivative yields more charged species in the network.</i>	58
<i>Figure 39: Evidence for electron donor functionality of the conventional polymer PVK (smoothed spectra).</i>	59

List of Tables

<i>Table 1: Peak data (IRAV) for photo- and doping induced infrared absorption and Raman spectroscopy of P3OT. T denotes translational modes and R denotes ring-bending modes.</i>	<i>43</i>
<i>Table 2: Peak data (IRAV) for photo- and doping induced infrared absorption of PDHT.</i>	<i>47</i>
<i>Table 3: Models, brands, performance and data of used equipment.</i>	<i>67</i>

1 Motivation

Most people who are asked for their opinion of what a polymer is, associate them with insulating properties. That is also what most polymers are used for. A few insulating examples are coatings of electrical cables to protect you from a shock when you connect the electrical outlet at home, or the chemical insulation, which makes some polymers perfect for usage in plastic gloves. Today, polymers have become much more than just insulators and new types of plastic materials have emerged, namely the conducting polymers. These belong to a larger class of materials, which researchers call synthetic metals. Following three statements [1] have motivated the last twenty years popularity of conducting polymers and the efforts carried out within the field:

1. *Conducting polymers are considered as new material with a large potential for new applications.*
2. *The systems of conjugated double bonds are subject to quantum chemical concepts and calculations. In that sense they are rewarding for theoretical modelling.*
3. *Certain excitations of solitonic nature in these organic materials are related to other disciplines, such as field theory, hydrodynamics, elementary-particle physics and some biological branches.*

1.1 Objective of thesis

In this study a materials research is presented with a physical investigation of photoexcited states in photoactive materials by use of various spectroscopic methods. Probable applications in future are in photovoltaics, for instance the utilisation of organic solar cells. Different polymer chain defects have been characterised theoretically and experimentally. All theory as well as corresponding experimental observations were carried out with respect to the ultrafast electron transfer process between donors and acceptors. Different doping techniques have been used in order to accomplish correct assignment of absorption features to the greatest possible extent. We have used the guest-host approach and present examinations of conventional polymer hosts with an embedded interpenetrating conjugated polymer/fullerene network forming the active guest layer.

In a further perspective the main objective and target is to appraise and perhaps present a clue to finding the optimum charge transfer system for future usage as active layer in the developing plastic solar cells.

2 Introduction

2.1 Overview of organic solar cells

A photovoltaic cell, or solar cell, is a device for harvesting the solar energy by converting the sunlight into electricity. Solar energy in form of photons that strike the surface of the cell releases charges, whose collection into an outer circuit is the basic phenomenon for the energy production. All solar cells, traditional inorganic as well as unorthodox plastic ones, consist of two or more thin layers. For inorganic solar cells, one of the limitations has been high production cost, because of necessary purification processes and the expensive ingot slicing methods where much of the material is wasted in saw cuts. A sad but evident fact for the developers is that the more efficient the material, the more costly. However, promising attempts are made to produce cheaper and efficient inorganic solar cells using for instance amorphous silicon or gallium arsenide.

Development of organic solar cells has only been carried out for a period of less than ten years, so it is a difficult task to predict their future at such early stage. If certain fundamental disadvantages of today's cells can be managed, especially concerning charge transport and degradation, organic solar cells have a good chance to succeed. Their decisive advantages compared to the inorganic will be low production costs, tandem structures that could yield very high efficiencies, superior processability and a better environmental compatibility. A whole polymer industry with know-how, financial resources, extensive knowledge and experience in thin film production is ready to realise plastic solar cells, as soon as the right photoactive systems and materials have been found. This is by far the most important advantage when it comes to the near future business potential of organic solar cells.

2.1.1 Operational description of the plastic solar cell

The operational principle of a plastic solar cell has many analogies to that of a natural green plant. Plants have developed a way of harvesting the solar illumination extremely efficient and the conversion into energy is called the photosynthesis. Operation of a plastic solar cell basically relies upon the ultrafast photoinduced electron transfer (see chapter 3.4) between a donor and an acceptor molecule.

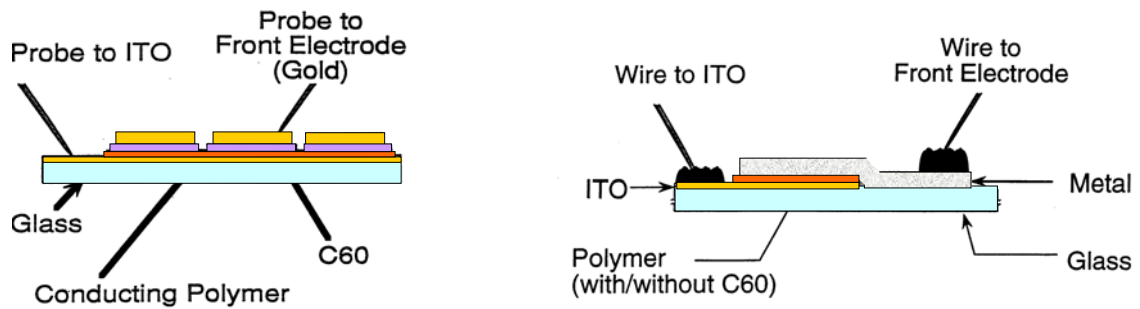


Figure 1: Comparison between a bilayer structure (left) and a bulk heterojunction structure (right) solar cell device.

For the case of inorganic semiconductor devices and silicon solar cells there is a well-developed formalism and modelling since decades. Same formalism and a qualitatively equal treatment can be applied for modelling and calculations of the operation of organic solar cells, although the physical reactions that govern the solar energy conversion on the molecular level are completely different. An organic solar cell like the one depicted below in Figure 2 consists of a comparatively small number of layers and is easy to produce, also in a laboratory without much specialised equipment. The transparent higher work function anode on glass or flexible plastic is irradiated by the sunlight, which excites the conjugated polymers in a donor-acceptor interpenetrating network and an exciton is created. This exciton is separated into two charges of which the negative electron is transported from acceptor to acceptor molecule towards the lower work function cathode and the positively charged and highly mobile polymer defect moves towards the anode. Hence, the charges reach their respective electrodes and are transferred into an outer circuit. A much more comprehensive description of this quantum solar energy conversion can be found in [2] but is not the aim of this work. For explanations of the used terminology, see chapter 3 in this thesis.

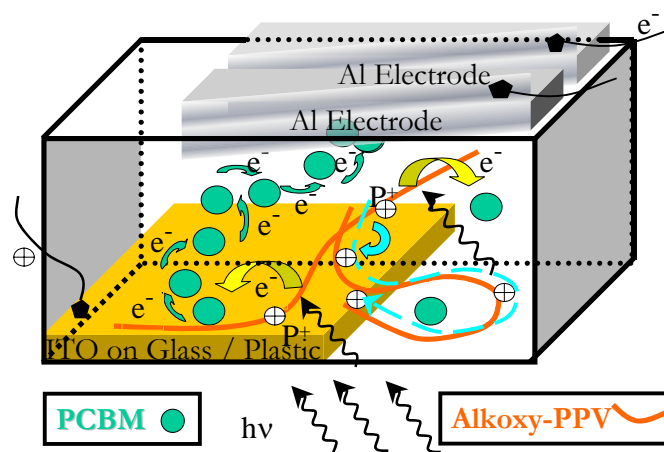
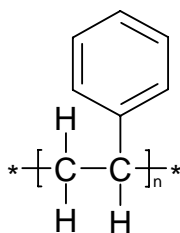


Figure 2: Main operational orders of an organic solar cell with an interpenetrating network structure.

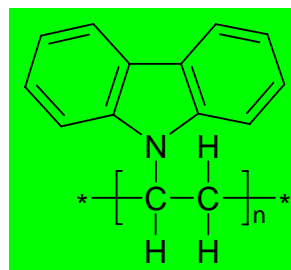
2.2 Polymers hosts

The main topic of this thesis is to investigate the physical properties of incorporated photoactive conjugated polymer/fullerene networks in conventional polymer matrices, also known as the guest-host approach. For this purpose, we have adopted a well-known method of embedding the active polymer substances by first dissolving them in an effective solvent and then producing a thin film. Important parameters to consider are of course the solubility of the hosts, but also the deterioration resistance when ageing and charge transport properties. For the investigation in this work, we have used four host materials which all of them contains sp^3 hybridised backbones unlike the conjugated guests. Drawn chemical structures of these conventional host polymers i.e. for polystyrene (PS), polycarbonate (PC), polyvinylcarbazole (PVK) and polyvinylbenzylchloride (PVBC) can be seen in Figure 3 below.

polystyrene (PS)



polyvinylcarbazole (PVK)



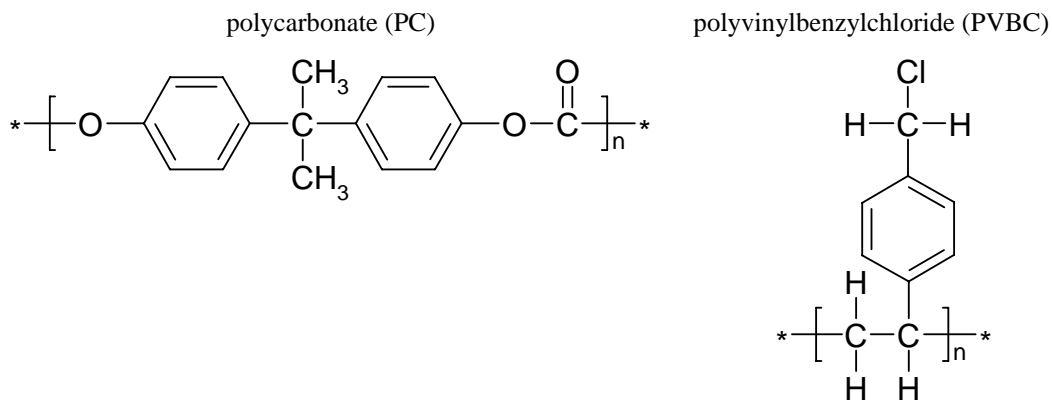


Figure 3: Host polymers for the embedding of photoactive guest materials.

There are several underlying reasons for attempting this guest-host approach.

- Embedding reduces problems with degradation at ambient conditions, as the conventional host component stabilises and protects the photoactive system from oxygen [3] and other environmental influences such as mechanical stress and wearing.
- An enhanced processability [4] of the composite blend due to the superior processing properties of the host polymer. Except for the processing, uniaxial stretching brings orientation of the guest and improves the physical properties of the conjugated polymers.
- Also an option of tuning the morphology [5] is supplied by the host. A certain distance between the involved parts optimises the performance of the charge transfer system. Adding a host material may control this parameter.
- Last but not least, additional charge transport properties of the host are introduced [6] in the active bulk heterojunction structure.

2.3 Polymer solutions

For film production reasons, the polymers must be dissolved in a good solvent and then cast on a suitable substrate. One of the crucial problems when producing a high qualitative polymer blend is phase separation of the involved components. In order to predict solubility or miscibility of polymers in solution it is necessary to consider the thermodynamics of it. From this point of view, a necessary but not sufficient condition for miscibility is:

$$\Delta G_{mix} = \Delta H_{mix} - T\Delta S_{mix} < 0$$

Here ΔG_{mix} is the free energy of mixing, ΔH_{mix} the enthalpy of mixing and ΔS_{mix} the entropy of mixing. The main consequence of this thermodynamic relation follows from the function $\Delta G_{mix}(x_I)$ where x_I is the molar fraction of component I . If this function is concave (less than zero) with no inflection points, we have complete miscibility over the whole range of compositions. At very low polymer concentrations we will always have miscibility but usually polymers show poor miscibility at higher concentrations. [7]

Also essentially immiscible polymers can be forced to form a finely dispersed system in different ways. Some of the methods are outlined below:

- Modification of the chemical structures by addition of functional side groups with convenient interaction characteristics, for example a functionalised derivative of buckminsterfullerene instead of its original symmetric structure (see Figure 17).
- Addition of a so-called compatibiliser, which is a block copolymer consisting of groups that are miscible with the other components of the blend.
- Promotion of interactions between the involved substances.

2.4 Conjugated polymers

Conjugated polymers became interesting in the end of the 1970's when it was discovered that doping could increase the conductivity of a polymeric material by many orders of magnitude [8]. Organic conductors from polyacetylene were produced with a certain weakness. There was a problem with an insufficient long-term stability in ambient environment of these new conducting polymers. Still, the future perspectives of conjugated polymers are very promising, but the applications are now rather in the field of photovoltaics and optical electronics than in large-scale low-tech production of organic conductors. For the photovoltaic industry these materials are promising and for development of organic displays, they show some unique electronic features. For the display industry especially the possibility of chemically designing them, which means to manipulate their electronic properties, for example by tuning the bandgap via small alterations in the molecular structure is attractive, as this could lead to easily adjustable colour emission of ordinary polymer LED's.

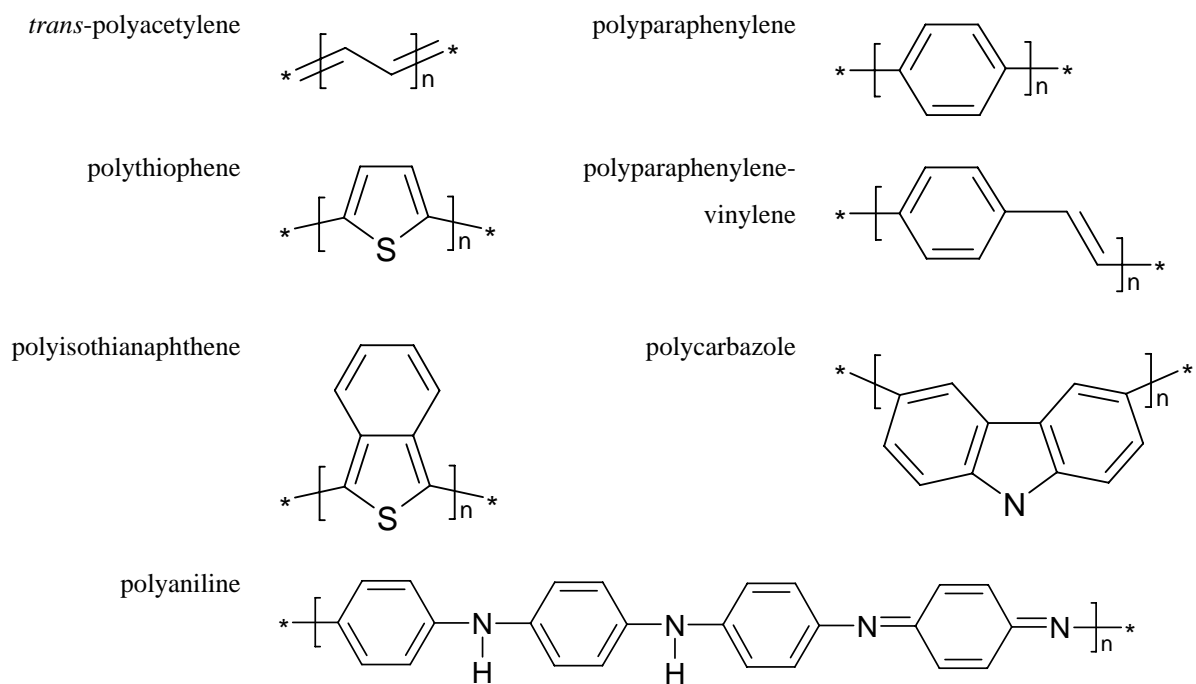


Figure 4: Names and chemical structures of common conjugated polymers.

3 Quasi-particles and electron transfer

This second theoretical part deals with the very core of this research field, namely with the charge carriers that give rise to conductivity in conjugated polymers.

3.1 Molecular structure

The distinguishing feature of all conductive polymers is the unsaturated carbon based alternating single and double bond structure of the polymer backbone, the so-called conjugated carbon chain. For simplicity reasons, the conjugated polymer *trans*-polyacetylene¹ will serve as model, as it has the simplest chemical structure of this group of materials. Its to some extent one-dimensional structure is held together by trigonal planar σ -orbitals between the carbon atoms in the backbone. Only three of the four valence electrons of carbon participate in this σ -backbone. This leaves us one remaining electron per carbon atom, which is located perpendicular to the trigonal plane in a p_z orbital. All these left over p_z orbital electrons from adjacent carbons, overlap and form the π -system. This can be described as a delocalised electron cloud with a periodic alternating density, which tempts us to speak about single or double bonds.

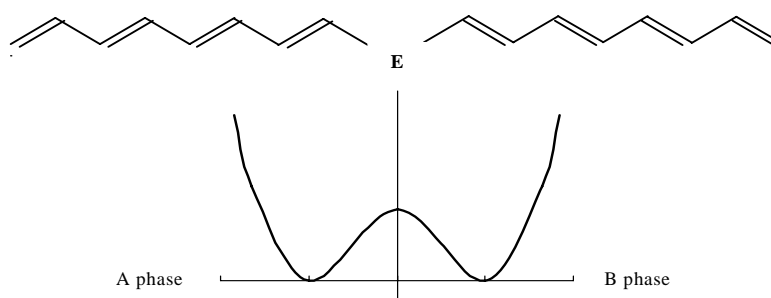


Figure 5: Structure of two equivalent *trans*-polyacetylene chains.

¹ The other isomer is called *cis*-polyacetylene, has a slightly different structure with non-degenerate ground state energy.

Since *trans*-polyacetylene has two equivalent structures, (A phase and B phase) with the identical ground state energy, it is called a degenerate ground state conjugated polymer, which is a specific property of this structure.

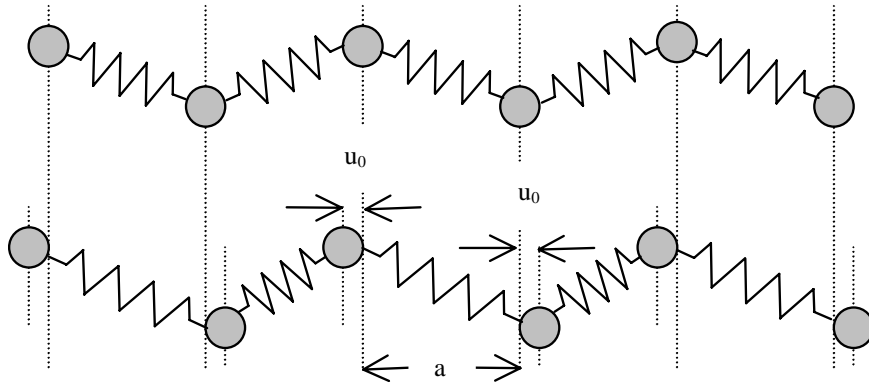


Figure 6: Polyacetylene chain before dimerisation (above) and after, (below). Modified picture from ref. [9].

The system of π -electrons delocalises along the carbon chain and this, together with the weak interchain interaction allows us to speak about the quasi one-dimensional nature of polyacetylene. Theoretical calculations show that if the single and double bonds were of equal length, the π -electron band would be half-filled by electrons due to Hund's rule and the polymer would be a metal. Peierls predicted that this can not be the case, because of instability of this structure against k_F phonons and the backbone dimerises into longer single bonds and shorter double bonds [10].

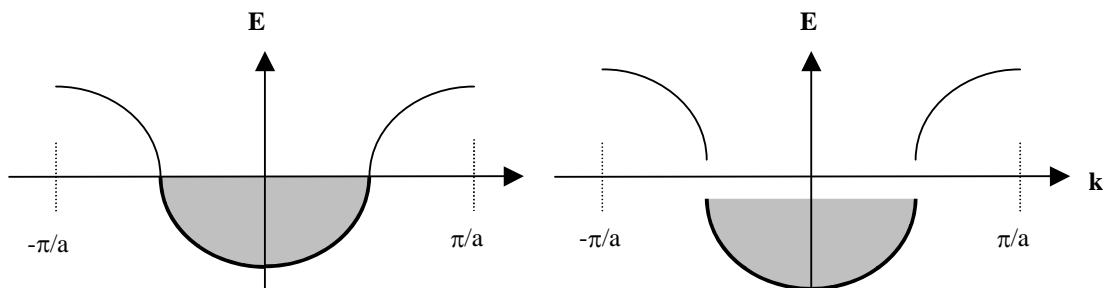


Figure 7: Transition from a metallic behaviour with half-filled π -band to a bandgap semiconductor due to Peierls distortion.

This is a spontaneous reaction and a decrease of the crystalline symmetry, which minimises the ground state energy of the occupied band. During this minimisation, the potential "string energy" of the dimerised polymer chain is increased and what we finally get is equilibrium

state, where the total energy of the polymer chain is lowered. The Brillouin zone reduces to half of the original length and occupies the range $-\pi/2a < k < \pi/2a$.

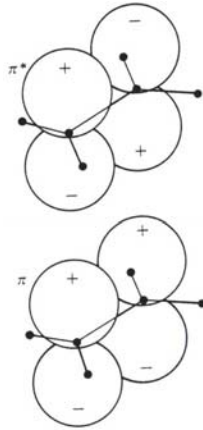


Figure 8: $\pi \rightarrow \pi^*$ transition in ethene. Picture from ref. [11].

This $\pi \rightarrow \pi^*$ allowed transition, which is depicted in Figure 8, is an asymmetric change of the dipole moment and a reduction of the bond strength as the electron is transferred from a bonding to an antibonding orbital.

3.2 Optical and electronic properties

Su, Schrieffer and Heeger have modelled infinite *trans*-polyacetylene chains theoretically (SSH-model) [12] and originally published this work in 1979. The model is applicable to one-dimensional carbon-hydrogen compounds with degenerate ground state energies. Electron-phonon coupling is taken into consideration, but the electron-electron interaction is neglected. Peierls' distortion predictions explain the development of two molecular bands, namely the π -band originating from highest occupied molecular orbital HOMO and the π^* -band originating the lowest unoccupied molecular orbital LUMO, with an energy gap between. We can calculate the size of this band gap E_g using the SSH-model, which leads to the following expression:

$$E_g = 8\alpha u_0$$

In the relation α symbolises the electron-phonon coupling and u_0 the dimerisation distance (see Figure 6). This means that because of the dimerisation, a transition from metal to semiconductor occurs. For an extensive review, see [13].

Also other models, for example the Pariser, Parr and Pople (PPP)-model [14][15] can be applied in order to describe the structure and to predict behaviours and properties of this class of materials.

3.3 Characterisation of excited states

When two *trans*-polyacetylene chains with different phases are put together, an obvious disturbance in the standard conjugation pattern occurs. The appearing bond alternation defect is known as neutral soliton. This kind of quasi-particle has an unpaired electron but is electrically neutral and is isoenergetically mobile along the polymer chain in both directions.

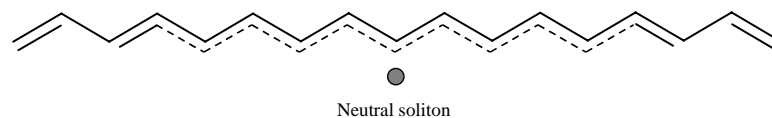


Figure 9: Neutral soliton in *trans*-polyacetylene.

This soliton gives rise to a state in the middle of the otherwise empty energy gap that can be occupied by zero, one or two electrons.

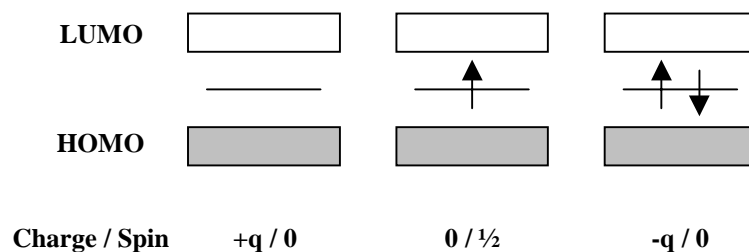


Figure 10: Three types of solitons. Note the reversed spin-charge relation.

If we look at the non-degenerate case instead of the degenerate ground state case a slightly different picture emerges. Most conjugated polymers have non-degenerate ground states since

their possible structures are not energetically equivalent. Examples of this are aromatic and quinoid forms of polythiophene as you can see in Figure 11.

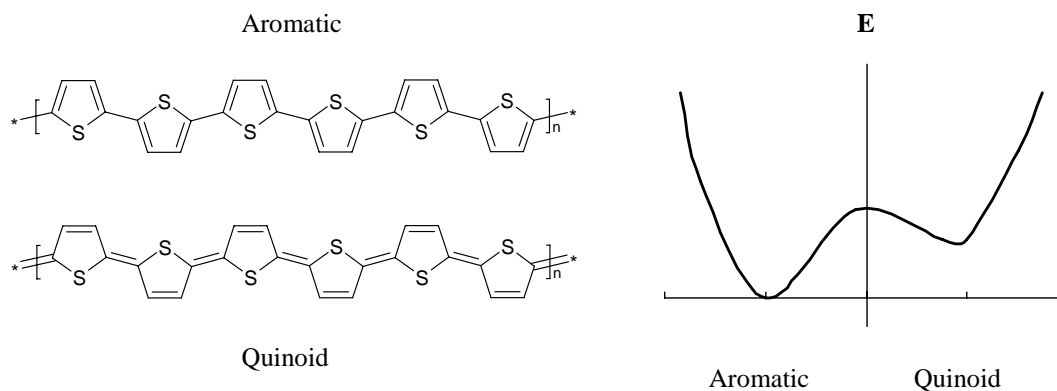
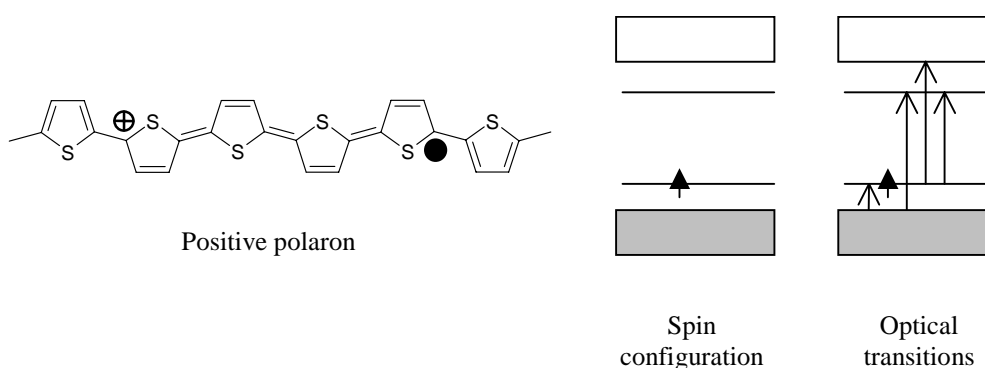


Figure 11: Lowest ground state energy is that of the aromatic form of polythiophene.

A number of different quasi-particles, called polarons, excitons and bipolarons are possible in non-degenerate ground state conjugated polymers. These quasi-particles give rise to new states within the forbidden bandgap and are observable via optical transitions with well defined energies. The extra energy required to change the bond alternation and increase the less energetically preferable quinoid structure provides the confinement potential that prevents the equal charges of bipolarons from separation. On the other hand, coulomb interaction between the charges hinders them from recombination and the state is equilibrium.



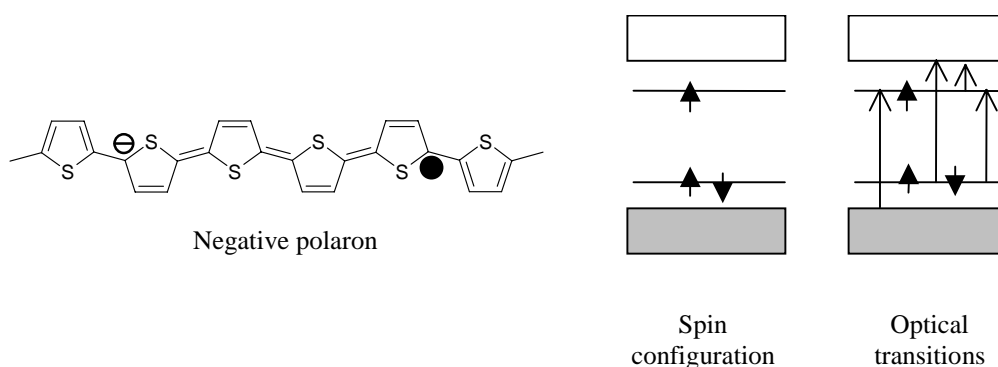


Figure 12: Structure, spin configuration and optical transitions for the positive and negative polarons.

Excitation of the polymer creates one electron and a hole on the chain. This effect is particularly important when the electron-hole interactions are strong. Coulomb attraction keeps them together and we consider the two opposite charges as a bound electron-hole pair. Excitons are denoted according to their delocalisation. If it is localised, it is called a Frenkel exciton and if it is delocalised, i.e. it extends over many molecular units we have a Mott-Wannier type of exciton.

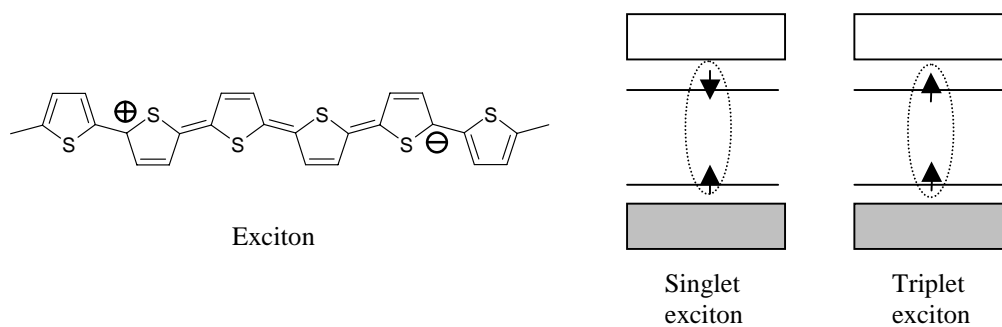


Figure 13: Energy diagram of the singlet and triplet excitons.

The exact nature of the primary photoexcitations in conjugated polymers is currently a matter of dispute in the scientific community. For an extensive treatment of this topic, I refer to a recently published book [16].

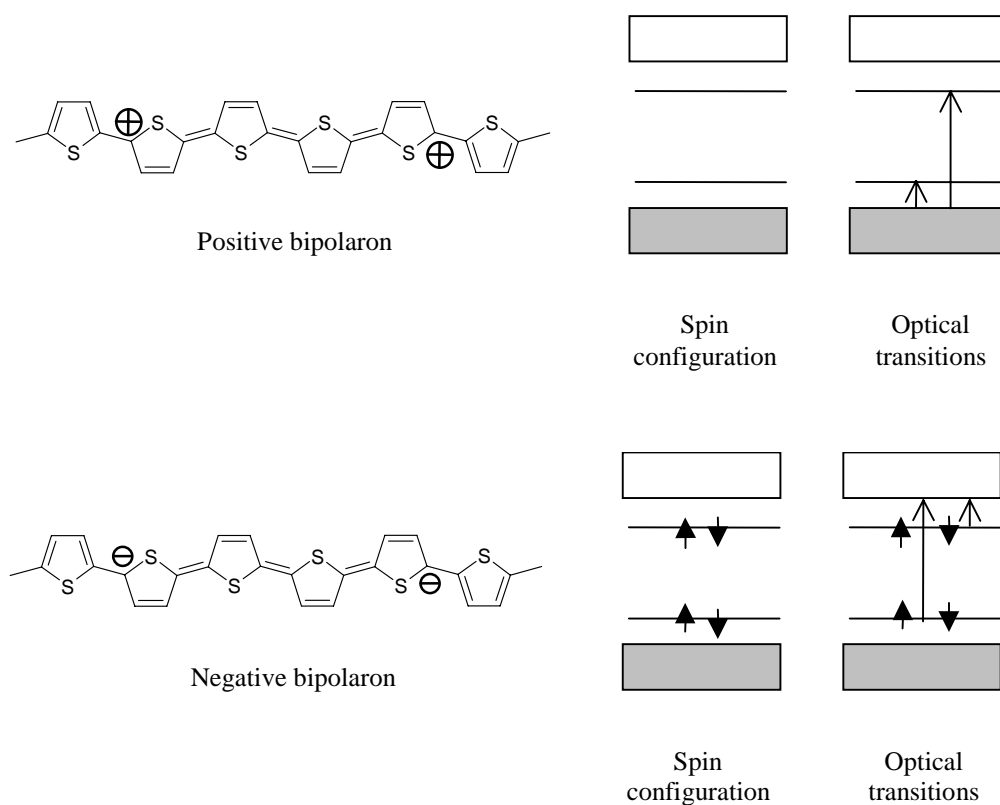
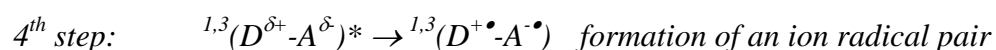
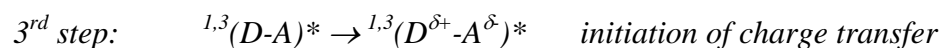
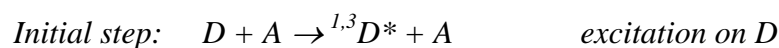


Figure 14: Structure, spin configuration and optical transitions for the positive and negative bipolarons.

3.4 Photoinduced electron transfer

Interdisciplinary research on charge transfer processes has been carried out for a long time. One hopes to be able to copy nature's sophisticated way of converting solar energy. The general outline of an intra- or an intermolecular photoinduced electron transfer can be divided into steps for a clearer understanding. Here the characters D , A are used for charge donor and acceptor and $1, 3$ denotes if the excited state is a singlet or triplet.





At each intermediate step, the process can relax back to ground state by releasing the energy in form of emitted radiation or as heat.

In step 3, the symbol δ is introduced. It denotes the fraction of charge transferred, continuously in the range between $0 < \delta \leq 1$, where $\delta = 1$ is the state where the whole electron has been transferred. For the formation of the ion radical pair in *step 4*, certain conditions must be fulfilled.

$$I_{D^*} - A_A - U_C < 0$$

These conditions regard the ionisation potential of the excited state of the donor, I_{D^*} , the electron affinity of the acceptor, A_A , and the attracting Coulomb force of the separated radicals U_C , including polarisation effects.

In the case of charge transfer from a polymer to a neighbour acceptor molecule, a stabilisation of the photoinduced charge separation (*final step*) is possible through carrier delocalisation on the cation radicals ($D^{+\bullet}$) (polarons) along the polymer chain and a structural relaxation of the anion radicals ($A^{-\bullet}$).

In 1992 Sariciftci and co-workers discovered the photoinduced electron transfer [17] from a conjugated polymer onto the new carbon form buckminsterfullerene C_{60} . The forward electron transfer from polymer to fullerene is ultrafast, less than one picosecond, and the back transfer inhibited. This strongly enhances the photoconductivity in polymers upon doping them with fullerene. It was later shown that this transfer occurred in a time-scale less than 300 femtoseconds [18].

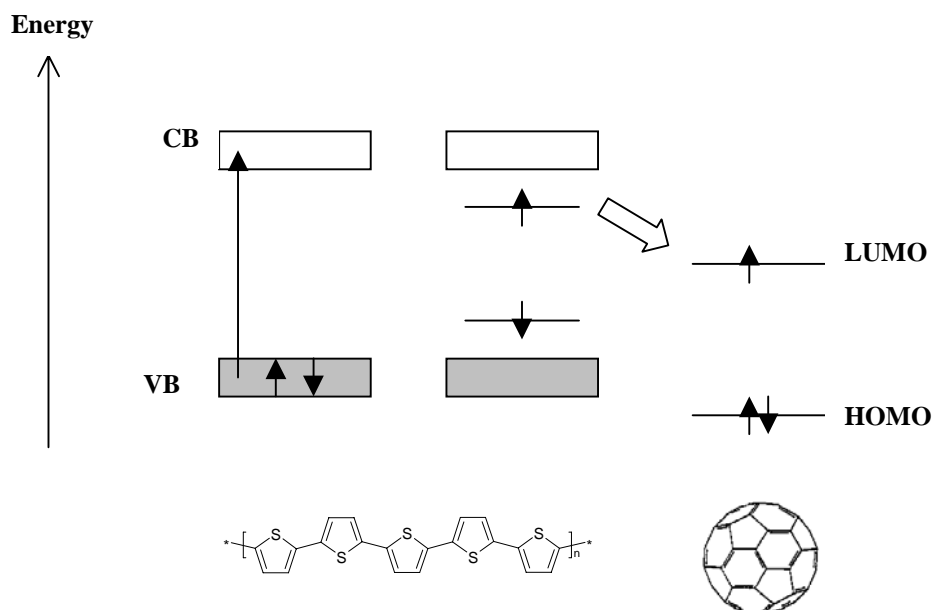


Figure 15: Schematic energy diagram for the ultrafast photoinduced electron transfer between a conjugated polymer and the buckminsterfullerene C_{60} .

After a photon has excited the conjugated polymer so that an exciton has been formed, the C_{60} accepts one electron due to its high electron affinity and establishes the anion C_{60}^- . What is left on the polymer chain is a cation radical, i.e. a positive polaron depicted in Figure 12, which is a mobile charge carrier that can move along the polymer backbone. As we see in the above energy diagram, this transfer is an exothermal reaction, where energy from the system is released.

3.4.1 Donors and acceptors

Certain manipulation of the conjugated polymer chain for enhancement of the solubility in organic solvents is necessary. This functionalisation of the conjugated structure can be achieved by introducing side groups like octyl- or hexyloxy-groups onto the polymer chain.

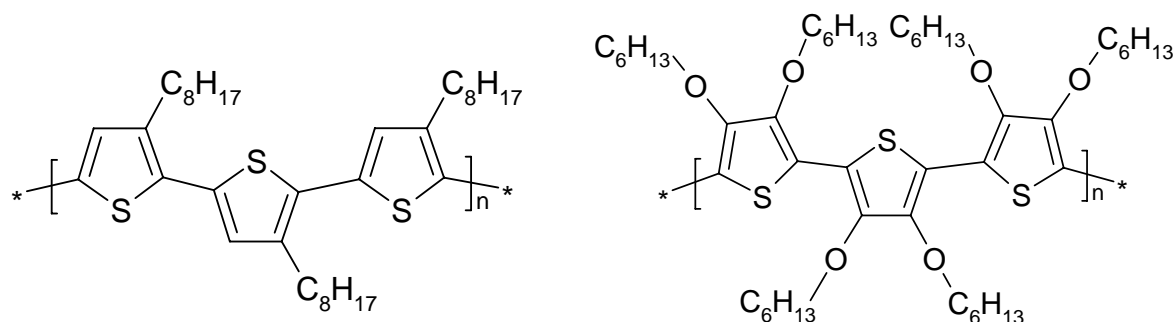


Figure 16: Two types of polythiophene derivatives used as donors in the work. Left the chemical structure of P3OT and right that of PDHT.

Throughout this work, the polythiophene derivatives poly(3-octylthiophene) (P3OT) and poly(3,4-dihexyloxythiophene) (PDHT) (see Figure 16) have been used as electron donors.

For the electron acceptance in the charge transfer system, an organic molecule with an interesting symmetric and almost spherical cage structure can be used. More in detail, the structure is that of a truncated icosahedron with one carbon atom in each point of intersection, altogether sixty carbon atoms. As a matter of fact, it is identical with the official FIFA² football although it is smaller. Since the C₆₀ structure was fully understood and explained by Kroto, Smalley and co-workers [19] in the 1980's, intensive research has been performed in a wide variety of fields, related to many different properties of the C₆₀ and future possible applications. Here, I will only describe those properties of fullerenes concerning their functionality as acceptors of electrons.



Figure 17: Left the symmetric structure of the buckminsterfullerene (C₆₀) and right the modified and functionalised derivative [6,6]PC₆₁BM.

² Fédération Internationale de Football Association

As we can see clearly above, the fullerene has an alternating single- and double bond structure along its equator just like the conjugated polymers. Here we see the sp^2 structure is not quite planar but arched around the centre of the sphere. If the molecular orbital levels of C_{60} are calculated using Hückel theory, we find that the LUMO (t_{1u}) has triply degenerate conduction band level and the HOMO (t_{1g}) likewise, on its corresponding energy level. C_{60} can accept as many as 6 electrons. Cyclic voltammetry experiments show distinct peaks which each one corresponds to C_{60} 's excellent capability of taking on six electrons [20]. Other experimental evidence for this has been found when doping with alkali metals [21]. This makes the molecule well suited to act as acceptor in a photoinduced electron transfer system. However, fullerene has a poor solubility in both polar and apolar organic solvents. To overcome this, synthesis of new fullerene derivatives with enhanced solubility with all desired properties maintained has been established. In Figure 17 one of these derivatives ([6,6]PC₆₁BM) is shown. This is the abbreviation of its full name 6,6-phenyl C₆₁-butyric acid methyl ester [22] and it was first synthesised in 1995.

4 Photophysics and infrared activity

This section consists of a brief introduction to spectroscopy and of an explanation of the origin of infrared activated vibrations (IRAV).

4.1 Life of photoexcited states

With a bit of fantasy, one can imagine striking similarities of popcorn to the lives of photoexcited states although another terminology is used for them. A more extensive description of the fate including birth, life and death of photoexcited states follow.

4.1.1 Absorption

Absorption spectroscopy is a method for determining what radiation energies can be absorbed by a sample. If the sample absorbs certain energy, species in it get excited in accordance to this energy. Molecular transitions from one energetic state to another occur. Many different transitions are induced and we speak about vibration, rotation and translation modes.

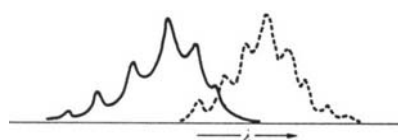


Figure 18: In the picture we see the mirror symmetry of the absorption spectrum (full line) and the emission spectrum (dashed line). Picture from ref. [23].

Absorption and fluorescence emission spectra have similar geometry due to the corresponding energy levels. Since non-radiative relaxation occurs within the electronic level, the spectra are separated along the energetic axis. The so-called Stoke's shift between the $0 \rightarrow 0$ transitions of absorption and emission (see Figure 20) arises because of intramolecular relaxation preceding fluorescent relaxation.

For all kinds of spectroscopy there are some basic background theories used in order to simplify the models describing the photophysical reactions occurring. The most fundamental of them is the Born-Oppenheimer approximation. Unless this approximation is made, the Schrödinger equation is not analytically solvable for a two- or more particle systems.

Generally speaking, this approximation compares the masses of electrons and the nuclei in a molecule. Since the mass of the electron is so small it does not affect the movement of the much heavier nuclei. We can consider the nuclei positions as fixed in our system.

Another very important principle that helps us to understand why some transitions take place and others do not is the Franck-Condon principle. Excitations of electrons in the molecule upon absorption of illumination change intramolecular forces that affect the nucleus, which starts to vibrate differently. The analysis of what vibrations are stimulated is

based upon the Born-Oppenheimer approximation where the nuclei are considered rigid.

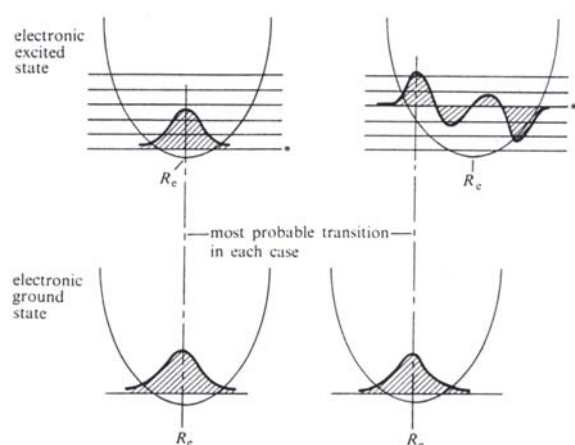


Figure 19: Electronic transitions according to the Franck-Condon principle. Picture from ref. [23].

The principle says that the nuclear conformation is adjusted after an electronic transition and not during it. When this is depicted like in Figure 19, it means that the allowed electronic transitions are vertical. For a transition, there must be an overlap between the wave equations of the electronic ground state and a vibronic level in excited electronic state. The larger the overlap, the more probable is the transition. This is the qualitative meaning of the Franck-Condon principle.

4.1.2 Relaxation

Excitation energy that has been absorbed by a molecule is converted into vibration, rotation or translation of neighbour molecules. This conversion can also be thermal under which the environment is heated. Apart from this thermal heating, another relaxation mechanism is deactivation of the excited state through dropping down from higher to lower energy levels. This decay is either a radiative reaction, where a photon is emitted or non-radiative at which the excitation energy is discarded otherwise.

Radiative relaxation mechanisms can be divided into the faster fluorescence emission between two electronic states of same spin degeneracy and the slower phosphorescence emission that occurs between states of different spin degeneracy. Several relaxation processes compete with each other and excitations always choose the fastest allowed way back to ground state.

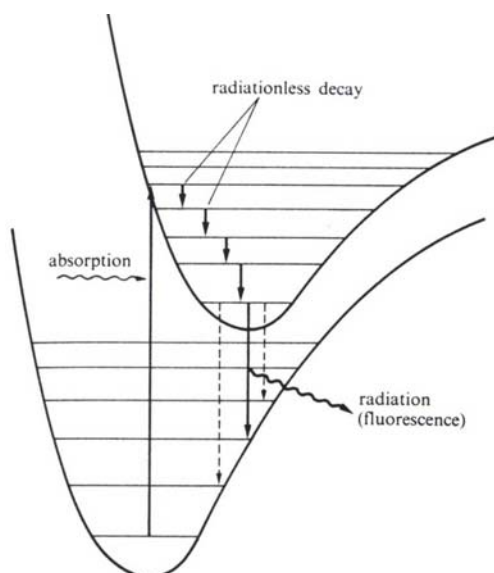


Figure 20: Electronic excitation followed by fluorescent relaxation. Picture from ref. [23].

Emission that is quenched, i.e. inhibited by another and more sufficient relaxation pathway often gives valuable information about charge- or energy transfers in various systems of nature.

To describe the various relaxation channels for an excited state the Jablonski diagram is illustrative. There we have two types of electronic energy levels with different spin characteristics, the singlet state with zero total spin and the triplet state with a total spin of one. Within the electronic levels there are a number of vibronic levels with less energy distances between each other in comparison with the electronic levels. As a consequence of the Pauli principle, each electronic energy level can be occupied by at most two electrons with opposite spins. When a molecule in its singlet ground state S_0 is excited, one electron is put onto an empty electronic state of higher energy. In case the spin is unaltered during this transition, the electron has reached another singlet state, for instance the S_1 level. Spontaneous emission from this level is the fluorescence emission. However, also internal conversions (IC) between overlapping wavefunctions of two vibrational states of equal energy although the electronic states are different are possible. This isoenergetic conversion is of course non-emissive.

Another conversion process is the intersystem crossing (ISC), which is a transfer from either higher to lower or between equal energy levels of the singlet to the triplet state. A molecule can relax non-radioactively down to the triplet ground state T_1 and from here return to the singlet ground state by emission of one photon. This is the phosphorescence emission

mechanism, which occurs in the relatively long time scale of ms to s and thus is much slower than the other relaxation mechanisms.

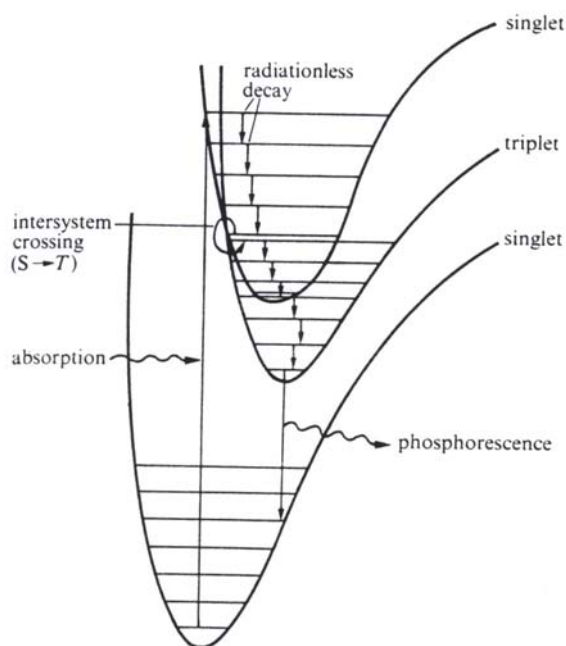


Figure 21: Jablonski diagram of intramolecular relaxation channels. Picture from ref. [23].

Investigations on charge transfer systems from conjugated polymers onto fullerene show strong quenching of the photoluminescence as well as intersystem crossing [4]. This implies strong influence of the acceptor molecules with high electron affinity on the photoactive system.

For this reason we can assume efficient competition of the ultrafast electron transfer with dipole allowed radiative and non-radiative relaxation channels.

4.2 Infrared activated vibrational (IRAV) modes

In our investigations, the sample is a thin polymer film in the solid state, which is probed by radiation in the infrared range. Throughout this work, special interest has been devoted to the new photoinduced states created under illumination of an excitation source and to their absorption. When additional charge carriers are introduced to the conjugated polymer chain by doping of any kind, they break the translational symmetry of the backbone structure. Tensions in the structure change the dipole moment of the polymer chain and new oscillatory modes, which are related to the translational degree of freedom, arise in the infrared energy range. Former symmetrical (Raman active) modes are activated and become visible with infrared spectroscopy. We have observed the infrared activated vibrational (IRAV) modes for all kinds of doping techniques.

A lot of theoretical work has been done in order to understand IRAV modes completely and how to attribute them right. For both *trans*- and *cis*-polyacetylene these attempts have been

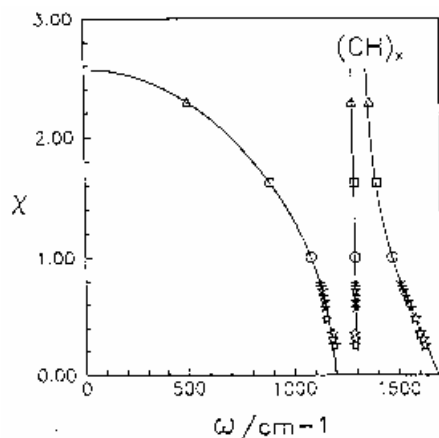


Figure 22: Plot of relative electric response χ versus energy, from ref. [32].

For the prediction of positions as well as intensity of the bands we make use of a plot (see Figure 22) of the electronic response χ (susceptibility or force constant) versus the energy. The IRAV modes that each one resembles a specific translation are added to the diagram and are scattered differently according to AM theory [31][32]. By doping of the materials we move the points of coincidence to various levels on the χ -axis along the slopes of IRAV modes. Open circles on the $\chi=1$ level denote pristine samples, open squares denote chemical doping and open triangles denote photoinduced doping and can be found on higher levels. This describes the shifts of the IRAV modes depending on the doping method. As the intensities of the peaks are qualitatively inversely proportional to the slopes of the modelled IRAV modes, also the intensity changes can be explained. IRAV modes are not allowed to cross over each other. The AM theory has not yet been extended to polythiophenes and it is not certain to what extent this can be applied for these materials.

Also Zerbi *et al.* has developed theories for interpretations of IRAV modes [33][34]. In comparison with AM theory, he uses the effective conjugation coordinate (ECC) theory with linear combinations of normal coordinates and the IRAV effects can be described in a similar way also with this formalism.

successful [32] and shifts and intensity changes of each IRAV mode can be predicted and fitted to models with good correlation.

5 Experimental

5.1 FT-IR set-up

A general outline of the experimental set-up is sketched in Figure 23 below³. The spectrometer is positioned on a stabilised table to avoid vibrations. The pump source consists of an argon ion laser situated in the neighbour room together with the chopper. The pump light is led through an optical fibre onto the actual FT-IR equipment.

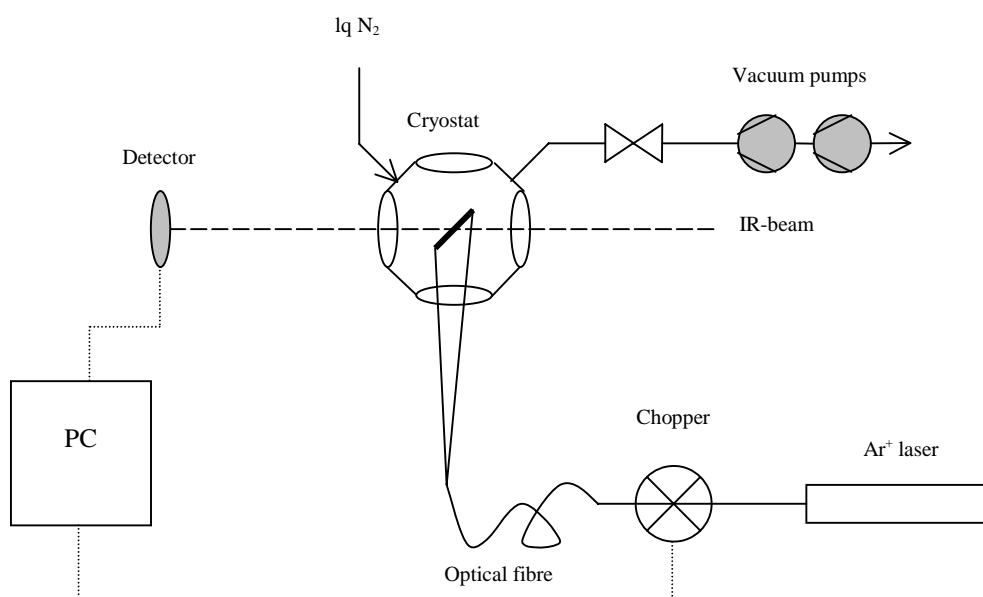


Figure 23: FT-IR set-up.

The sample was mounted on a cold finger on the from four directions optically accessible liquid nitrogen cryostat, which was evacuated by two pumps. Zinc selenide windows were used due to its optical transmittance in the infrared. The evacuation pumps are a rotation vacuum pre-pump and a turbo molecular pump, which serves as the high performance device and enables pressure of less than 10^{-5} mbar. Thermal stabilisation was awaited before measurements began.

³ A more detailed list of used devices and their specifications can be found in the appendix, last in this work.

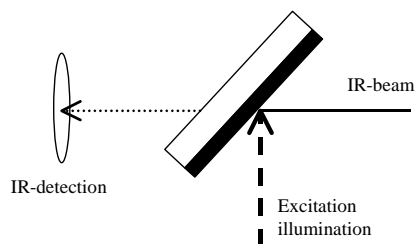


Figure 24: Excitation of cast pellet sample and the detection of transmitted infrared probe light.

Transmission of infrared probe light was measured during a repeated excitation with the light on, followed by dark scanning process. Detectors were either the liquid nitrogen cooled MCT type (mercury cadmium telluride) or the less sensitive DTGS type (deuterated triglycine sulfate) detector.

5.2 Sample preparation

For the FT-IR spectroscopy measurements all active substances have either been incorporated into or coated on potassium bromide (KBr) pellets, zinc selenide (ZnSe) or germanium (Ge) substrates. Thin film samples were produced using drop cast or spin cast techniques and the best film qualities were obtained when evacuation of the drop cast samples was carried out immediately after coating. Solutions of one weight percent pure polymer constituent dissolved in the polar solvent *ortho*-dichlorobenzene (ODCB) were used as base.

5.3 Measurement modes

Absorption in the IR range as been measured for three types of doping of the samples. Those measurement modes are photoinduced doping, chemical and electrochemical doping.

5.3.1 Photoinduced absorption

The conjugated polymer chains were excited by illumination of light with photon energy exceeding the size of the bandgap. We mostly used excitation energy in the blue-green range (488 nm) of the argon ion laser. This illumination yield localised and delocalised chain defects in the structure that give rise to the new states in the bandgap. When using the same formalism as in semiconductor physics we can describe this absorption in analogy with p doping although they were all induced by illumination of light. This method is a clean way of injecting charges onto the polymer chain, which is an advantage for well-defined characterisation. Standard measurements consisted of 6000 consecutive scans with an alternating external pump source with 10 seconds of light on (30 mW/cm^2) scans followed by

10 seconds of dark scans. Measurements were carried out in liquid nitrogen temperature of around 80 K and vacuum (less than 10^{-5} mbar).

5.3.2 Chemically doping induced absorption

For chemical doping, a thin film coated on a ZnSe substrate or a KBr pellet was exposed to iodine vapour during a few minutes. The ultra weak doping was performed in a tight vessel with a few evaporating iodine grains on the bottom, where the substrate coated with conjugated polymers was mounted a short distance above the bottom of the vessel. After a careful heating of the grains for only a few minutes, iodine molecules were incorporated as strongly reacting agents within the film. Stronger chemical doping (weak and strong) was obtained with a simplified attenuated total reflection spectroscopy element (miniATR) where the density of the iodine vapour is considerably higher.

5.3.3 Electrochemically doping induced absorption

Electrochemical doping is a strong method where very high degrees of doping can be reached. Reversibility of the doping reaction is achieved just by changing the electrode potential. With the attenuated total reflection element (ATR) [24], *in situ* electrochemical processes can be studied. For this method a three-electrode electrochemical cell was used. Working electrode, counter electrode and reference electrode consisted of a Ge reflection element coated with a platinum (Pt) layer, a Pt foil, and a silver/silverchloride (Ag/AgCl) wire, respectively. The electrolyte solution used was 0,1 M TBABF₄ (TetraButylAmmoniumBF₄) in acetonitrile.

5.4 Improvements of the measurement system

A new chopper system has substituted the former one. Through software control of this system, the chopping frequency can be changed and thus optimised. To eliminate harmful back transients that might damage the spectrometer, the system suppresses these transients. A thermo element was mounted on the sample for temperature control. For luminescence and absorption spectroscopy with samples of various shapes, new holders were constructed that simplified mounting and measurements.

5.5 Qualitative to quantitative values

In this study samples of various qualities and materials are compared to each other. In order to get comparable values it is important to normalise the spectra. Another desire is to obtain quantitative data about the number of excitations in a sample. The following derivations of a normalisation method quantification method serve our purpose and are approximations of the reactions that occur during the photoinduced absorption spectroscopy.

Unless the sample is thick enough to absorb all excitation energy there will be a film thickness dependence of the measured absorption. This influence must be taken into consideration and we apply Lambert-Beer's law of absorption on our sample. The photoinduced absorption spectra (PIA) were corrected the following way [24]:

$$\text{corrPIA} = \frac{PIA}{A(\lambda_{exc})} \quad A(\lambda_{exc}) = \frac{I_{abs}}{I_0} = 1 - T(\lambda_{exc}) \quad T(\lambda_{exc}) = 10^{-OD(\lambda_{exc})}$$

Optical density OD at the excitation wavelength λ_{exc} is a product of the absorption coefficient α and the film thickness z , which will be used later. Combination of the three expressions above yields the correction term for the photoinduced spectra in order to get comparable values.

$$\text{corrPIA} = \frac{PIA}{1 - 10^{-OD(\lambda_{exc})}}$$

After this normalisation of a spectrum we turn our attention towards the quantification of it. Is there a relation between the fractional change in transmission ($-\Delta T/T$) and the changes in probe absorption coefficient due to the created excited states? The answer is yes and the approximation the following:

We begin with the crude assumption that both the incident probe light and the pump light is radiated along the z -axis and reflection and scattering on the sample can be neglected. Then the light intensity I can be expressed as

$$I(z) = I_0 e^{-\alpha z}$$

If the absorption depth L within the sample declines exponentially according to Lambert-Beer and there is a proportionality between the number of excited states and pump light intensity, we can express the density of populated excited states with respect to the depth $N(z)$ as

$$N(z) = N_0 e^{-(L^{-1}z)}$$

Now we can estimate the fraction of absorbed probe photons in an infinite thickness dz when we introduce the absorption cross-section of the probe beam σ .

$$\frac{dI}{I}(z) = [-\alpha z - \sigma N_0 e^{-(L^{-1}z)}] dz$$

This gives the logarithmic transmission of the probe beam through the sample after integration over the whole depth ($0 \rightarrow D$):

$$\ln T = \ln \frac{I_D}{I_0} = -\int_0^D [\alpha z + \sigma N_0 e^{-(L^{-1}z)}] dz$$

From this we obtain the final relation that describes the change in transmission of the probe due to the pump source. The z dependence anneals when we consider only the normalised fraction.

$$\frac{T - T_0}{T} = \frac{\Delta T}{T} = \exp[-\sigma N_0 L (1 - e^{-L^{-1}D})] - 1$$

We arrive at an expression, which can be analysed in two ways depending on the nature of our samples. For the case of a thin film in comparison with the absorption depth of the pump light ($D \ll L$) and small transmission changes ($\sigma N_0 D \ll 1$) we have the following proportionality:

$$-\frac{\Delta T}{T} \approx (\sigma N_0) D \quad (D \ll L)$$

For the other case when the thickness of the sample is large in comparison with the absorption depth of the pump source ($D \gg L$) and the transmission changes remain small we obtain another proportionality. This is the case for all measurements and all samples in this study.

$$-\frac{\Delta T}{T} \approx (\sigma N_0)L \quad (D \gg L)$$

We now have derived a relation between the photoinduced absorption spectrum and the changes in absorption coefficient. This relation enables us to evaluate the spectra not only qualitatively, but also quantitatively.

6 Results and discussions

Results of the spectroscopic studies on poly(3-octylthiophene) (P3OT) and poly(3,4-dihexyloxythiophene) (PDHT) pristine or doped and either with or without acceptors embedded in different host surroundings are presented and discussed in this section. Also the morphology of thin film structures is discussed.

6.1 Comparative doping studies

6.1.1 P3OT

When we study the infrared spectra for doped P3OT we distinguish the IR/V bands as a number of more or less well defined and resolved peaks.

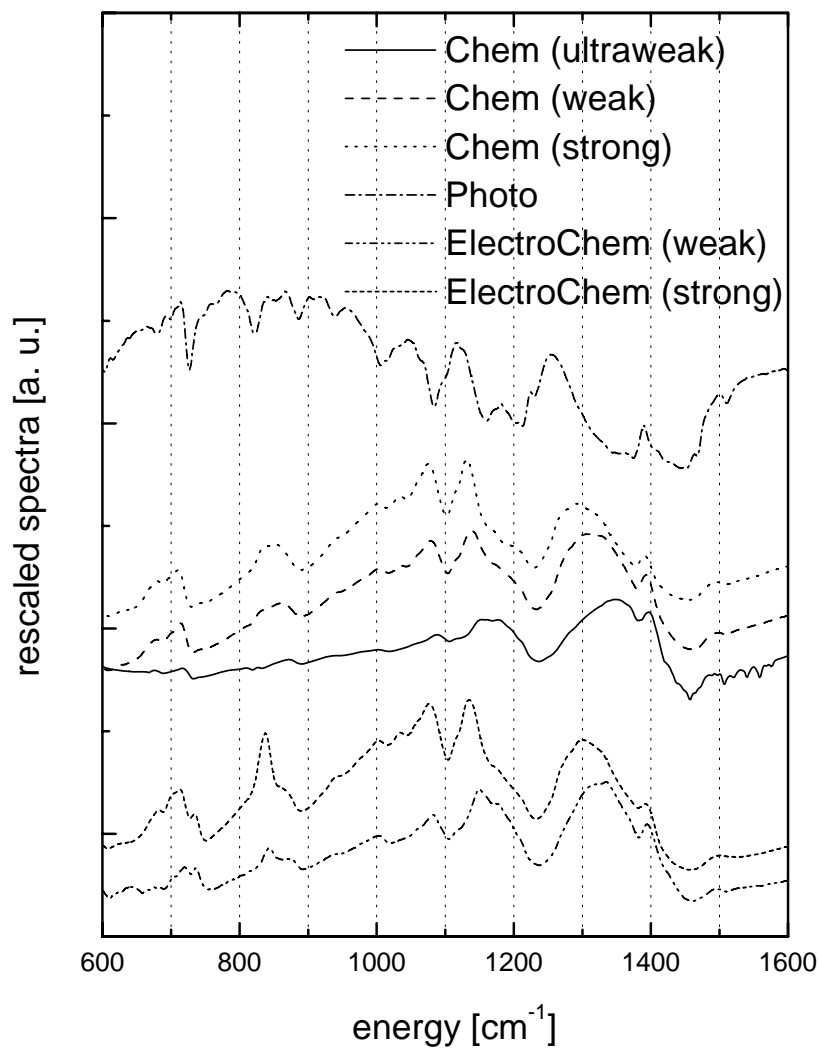


Figure 25: Comparison of IR spectra of P3OT for different doping techniques and levels.

The photoinduced spectrum shows IRAV bands ranging from 1100 to 1600 cm^{-1} . These peaks are positive and their exact positions are tabulated below. In the lower energy range ($\sim 800 \text{ cm}^{-1}$) there is a background signal in which the IRAV modes consequently are difficult to assign. In this regime, we can not say whether the bands are positive or negative. This strong background signal only exists for the photoinduced doping technique and is absent for the other doping induced spectra.

In order to assign these observations as correct as possible we compare them with data measured by other groups. Uncertainties due to quality differences of materials are inevitable, but anyway the comparisons can be regarded at least as guidance. When we compare with low

doping Raman spectroscopy measured on P3OT, [26] the spectra are comparable down to 1100 cm^{-1} but further down in energy the resemblance decreases. The strongest bands at 1442 , 1376 and 1182 cm^{-1} are assigned to various stretching modes of the thiophene ring, symmetric, intraring and interring respectively. When we compare those positions with our own spectra, we see a strong shift to lower energies for these.

<i>Mode</i>	<i>Photo</i>	<i>Chem.</i> (<i>S</i>)	<i>Chem.</i> (<i>W</i>)	<i>Chem.</i> (<i>UW</i>)	<i>E-chem.</i> (<i>S</i>)	<i>E-chem.</i> (<i>W</i>)	<i>Raman</i> [26]	<i>Lit.</i> [33]
R ₁	593	590	594					594
R ₂	689	676	676	680	682	683		687
R ₃	712	712	715	721	712	718	728	717
R ₄	796	846	858	867	837	846		800
T ₁	1047	1075	1080	1090	1078	1084		1047
T ₂	1118	1134	1137	1161	1134	1152	1182	1119
T ₃	1181	(1194)						1182
T ₄	1255	1292	1312	1351	1301	1327	1376	1254
T ₅	1391	1396	1396	1398	1396	1398	1442	1393

Table 1: Peak data (IRAV) for photo- and doping induced infrared absorption and Raman spectroscopy of P3OT. T denotes translational modes and R denotes ring-bending modes.

Lee *et al.* has performed similar studies [27] and by applying the same interpretation and formalism [28] on our results we get following picture. In the upper range (1100 - 1600 cm^{-1}) we see clear positive peaks that according to this model can be associated with the uniform translation of the positive charges (polarons) at the energies 1047 , 1118 , 1181 and 1255 cm^{-1} . These are called the T₁ to T₄ modes. We assign the T₅ peak at 1391 cm^{-1} with non-uniform oscillatory translation of the polaron on the polymer chain. In the lower energy range the bands are less defined and speculative. Nevertheless we distinguish vague features at 593 , 689 , 712 and 796 cm^{-1} , due to a weak coupling of the charges to the thiophene ring which is exposed to a slight distortion by bending. These are called ring deformation modes R₁ to R₄ using the same formalism. Apart from the lowest energy range where evaluations are ambiguous, we have obtained experimental results that are very close to those obtained by Lee *et al.*

The strong background signal mentioned before below 1100 cm^{-1} may be due to persistent charges trapped in the sample over a longer period of time. These could explain the negatively looking band features in this low energy range. A way of overcoming these would be to scan first in the dark and then constantly illuminate the sample while scanning. Unfortunately this technique has worse signal to noise properties and is sensitive to changes during the necessary long-term measurement. Also heating of the sample by illumination may have influence in this background signal. Time resolved photoinduced absorption for prompt signal investigations is suggested for further work on this topic.

There is an astonishing conformity and correspondence between the IRAV modes of different doping techniques. Every single peak in the upper range can be seen in each spectrum. The positions are shifted to lower energies (red shifted) for the photoinduced spectrum in comparison with doping induced spectra. This is a typical feature for conjugated polymers and can be explained in detail by the amplitude mode formalism (AM) [28][30] and later extended versions of it. [31][32] Another unambiguous spectral detail is the peak shifts for different degrees of chemical and electrochemical doping. The stronger the doping level, the further red shifted IRAV peak. One suggestion for this behaviour is the enhanced electrical conductivity by doping that shifts the peaks to the lower energies. For clarity, all IRAV data [cm^{-1} units] are collected in Table 1. Literature data are denoted *Raman* and for photoinduced doping *Lit.*

In the extended range depicted in Figure 26, we see clear differences between absorption spectra of various doping techniques. When we draw attention to the photoinduced and the chemically doping induced spectra, we see the polaron feature for the photoinduced spectrum is shifted more than 2000 cm^{-1} to lower energies. Also the geometry of the peak is another. This extended regime does not show the similarities between different doping methods as the lower infrared range did.

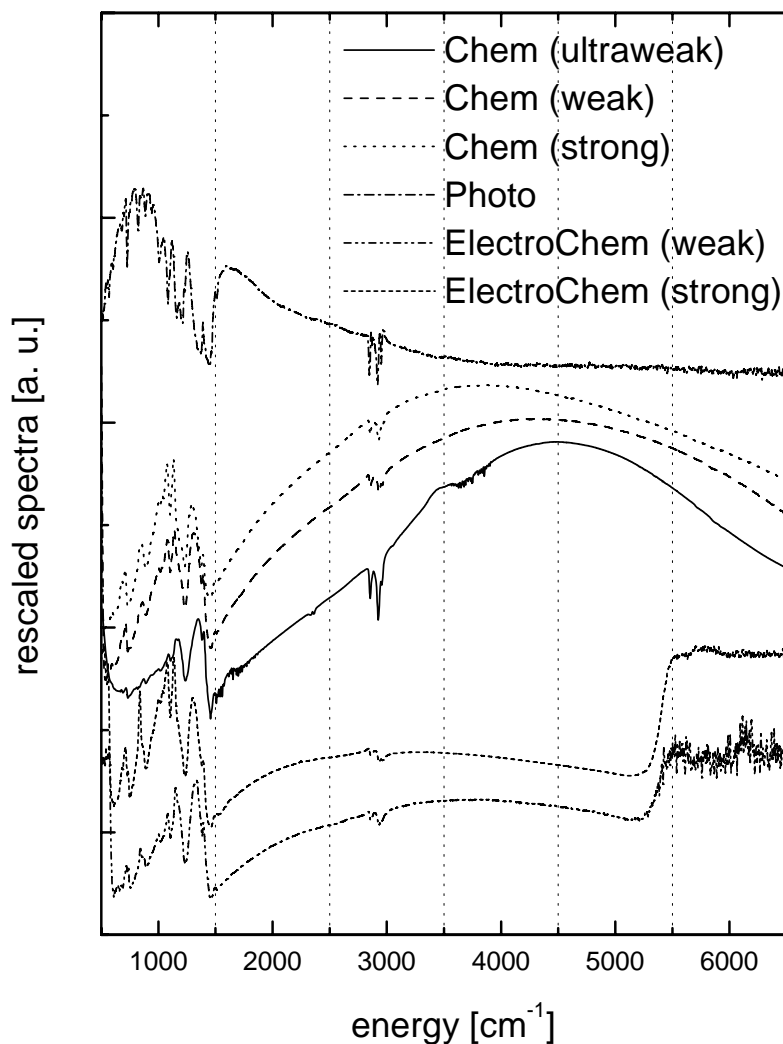


Figure 26: Comparison of doping induced absorption for P3OT over an extended energy range.

6.1.2 PDHT

The same doping experiments have been carried out for PDHT. Very little is published about this material and the assignment of its IRAV modes is carried out in close accordance to the former one for the case of P3OT. In order to find the photoinduced IRAV modes of the pure PDHT sample also consideration was taken to spectrum with acceptors. This improved the resolution and definition of peaks compared to the pure PDHT sample spectrum, which has a very weak signal and therefore is more influenced by noise.

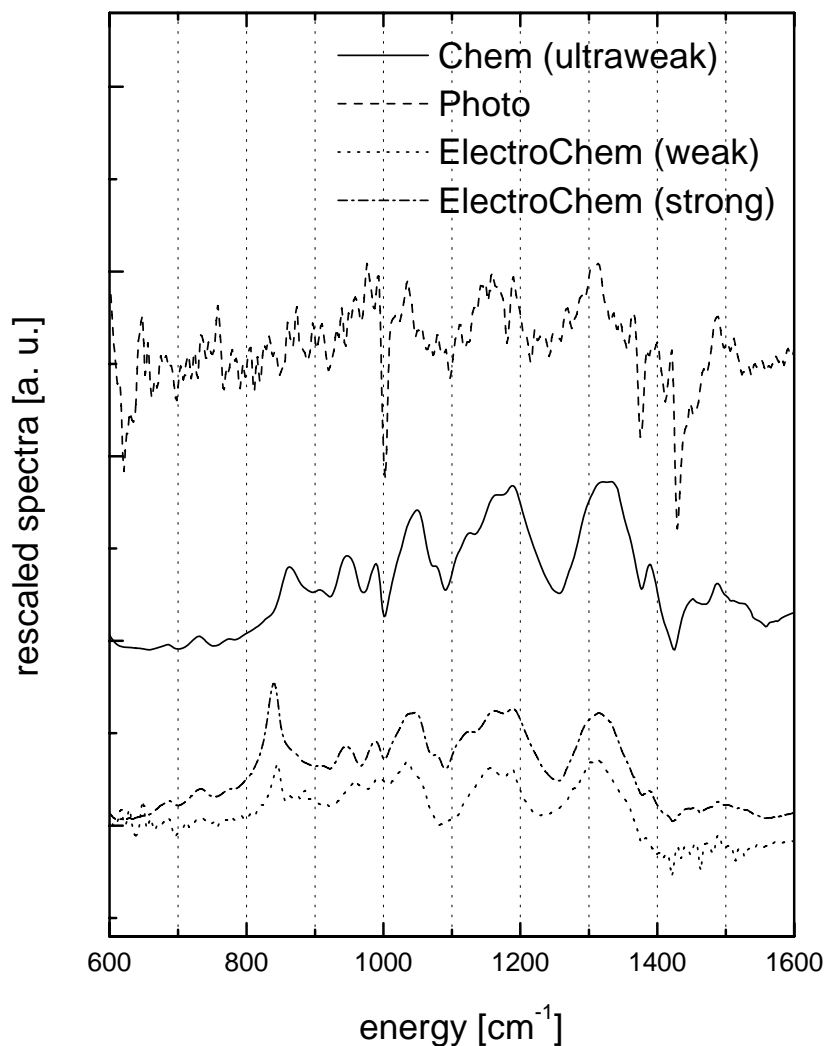


Figure 27: Comparison of IR spectra of PDHT for different doping techniques.

A description of what we see is a weak signal to noise photoinduced absorption spectrum with less disturbance of the background signal compared with P3OT. Here we see positive IRAV bands also in the energy range below 1100 cm⁻¹. Neither the red shift of the photoinduced spectrum with respect to the others, nor the dependence of doping degree is particularly pronounced for this material. The shift of the photoinduced spectrum is still there, but much more insignificant as for P3OT. Due to the lack of published characteristics of PDHT we can not compare these spectra with other relevant data.

If we choose to make an interpretation analogous to that for P3OT based on Lee *et al.* anyway, the following picture comes up. Assignment of ring bending IRAV modes in the low energy range is not certain. We can assign the following four modes to uniform translational motion at 1035, 1145, 1190 and 1312 cm^{-1} , T₁ to T₄. The last oscillatory vibration, which we call T₅, can only be seen for the chemical and electrochemical doping at around 1390 cm^{-1} . As for the P3OT case, all data [cm^{-1} units] available are collected in the following table.

<i>Mode</i>	<i>Photo</i>	<i>Chem. (UW)</i>	<i>E-chem. (W)</i>	<i>E-chem. (S)</i>
		732		730
	(869)	864	843	839
	(957)	945	954	945
	(995)	989	989	989
T1	1035	1047	1035	1041
T2	1145	1123		1126
T3	1190	1187	1187	1190
T4	1312	1327	1312	1315
T5		1391	1388	1388

Table 2: Peak data (IRAV) for photo- and doping induced infrared absorption of PDHT.

The extended energy range spectra for PDHT have been smoothed because of very high noise, especially for the photoinduced absorption spectrum. All spectra in Figure 28 have been roughly averaged over around 200 cm^{-1} , but we still see strong noise features in the spectra above 4500 cm^{-1} .

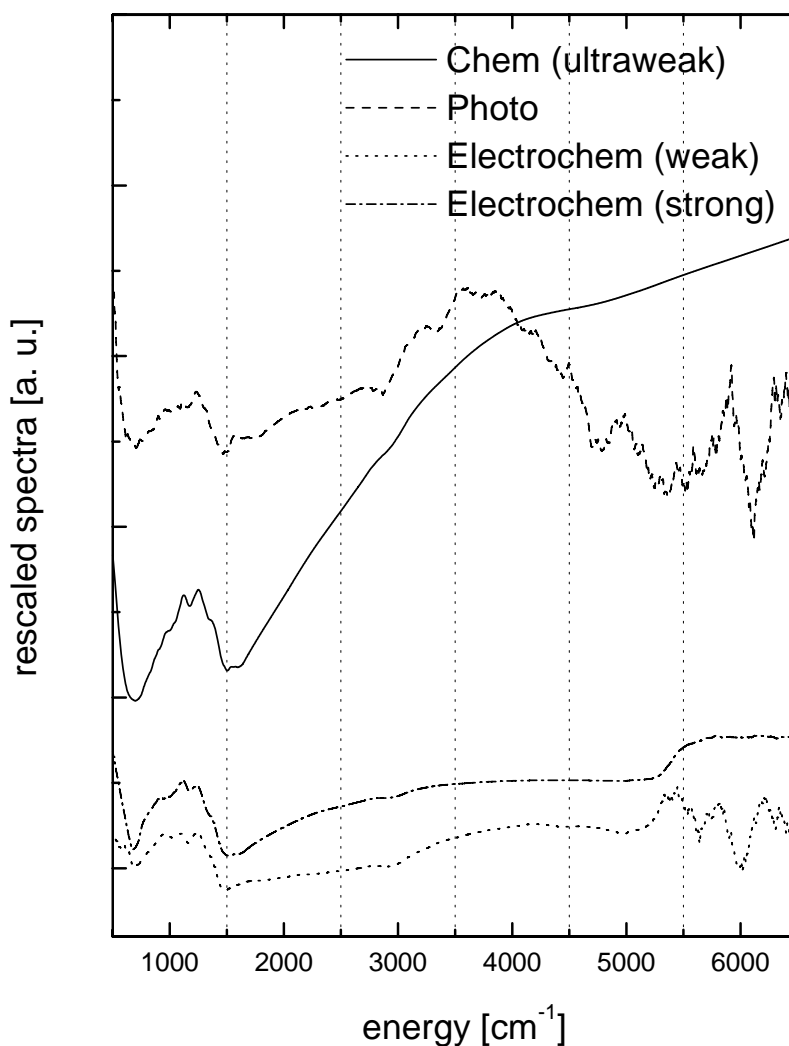


Figure 28: Comparison of doping induced absorption for PDHT over an extended energy range (smoothed spectra).

6.2 Photoinduced absorption for donor/acceptor networks

The photoinduced absorption spectra change considerably upon adding an acceptor substance to the thin film. We added the fullerene derivative [6,6]PC₆₁BM, depicted in Figure 17 and called PCBM in the following, to the pristine conjugated polymers and measured the photoinduced absorption. Upon addition of a comparatively high weight fraction (1:1 ratio) of acceptor molecules into the polymer compound, we create a bulk heterojunction donor-acceptor network. This enhances the infrared activity by at least a factor of five without shifting the energetic positions of the photoinduced absorption peaks. This can be seen in Figure 30. Responsible for this enhanced behaviour is the ultrafast photoinduced electron

transfer that draws electrons away from the polymer chain and leave an increased number of positive polarons on the backbone, which gives rise to enhanced IRAV intensities. Hence, this process governs a sufficient suppression of recombination, which increases their lifetime. Summarising this yields an increased number of polarons that live longer, which leads to a remarkable enhancement of the infrared absorption signals we obtained by spectroscopy.

When we study the spectra of P3OT in comparison with P3OT/PCBM we see the features described above. The broadest peak with maximum at around 1800 cm^{-1} is due to the lowest energy transition of the positive polaron. Its broad appearance originates in the transition from the π -energy band to the lower polaron level.

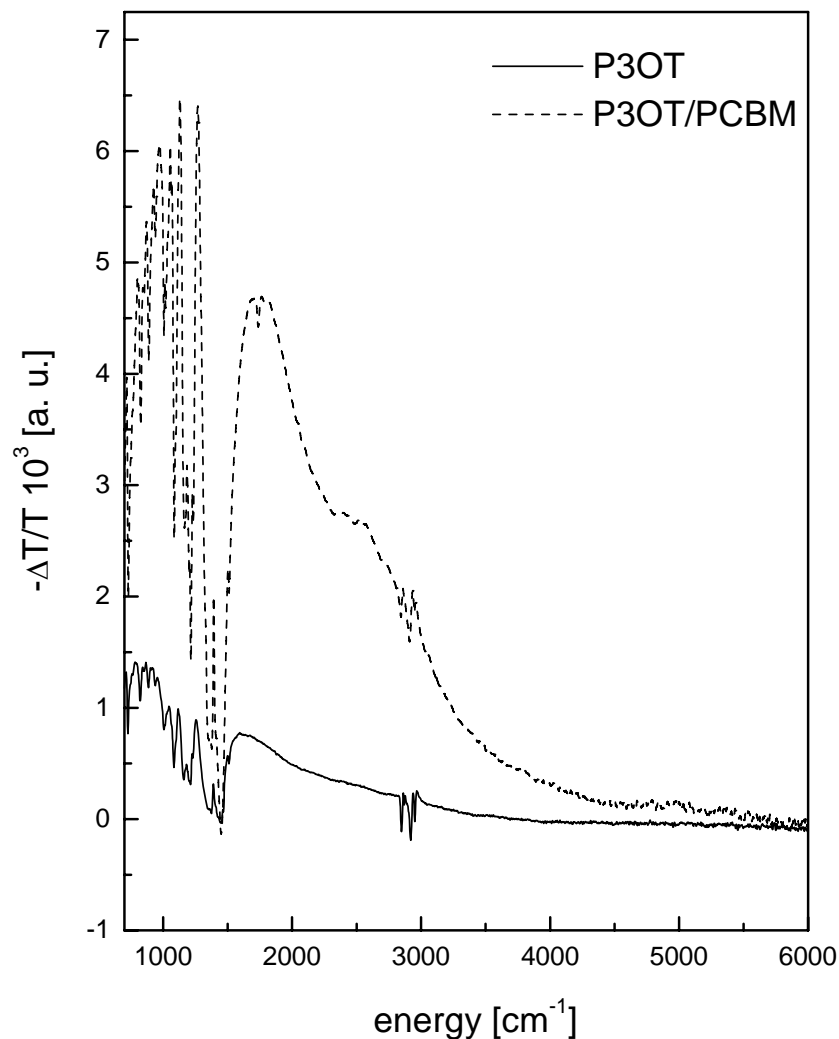


Figure 29: IR electronic absorption for P3OT with and without acceptor molecules within the network structure.

This polaron peak has a full width at half maximum (FWHM) of around 1000 cm^{-1} and ends at 1500 cm^{-1} where the IRAV modes begin. Both polaron band and IRAV modes are well correlated between films with and films without acceptor molecules and no shifts occur in the spectra. A feature that looks like a shoulder is seen on the upper energetic side of the electronic transition only for P3OT/PCBM. For both spectra in Figure 29, we see bands just below 3000 cm^{-1} due to stretching of hydrogen bonds of CH_3 or CH_2 groups.

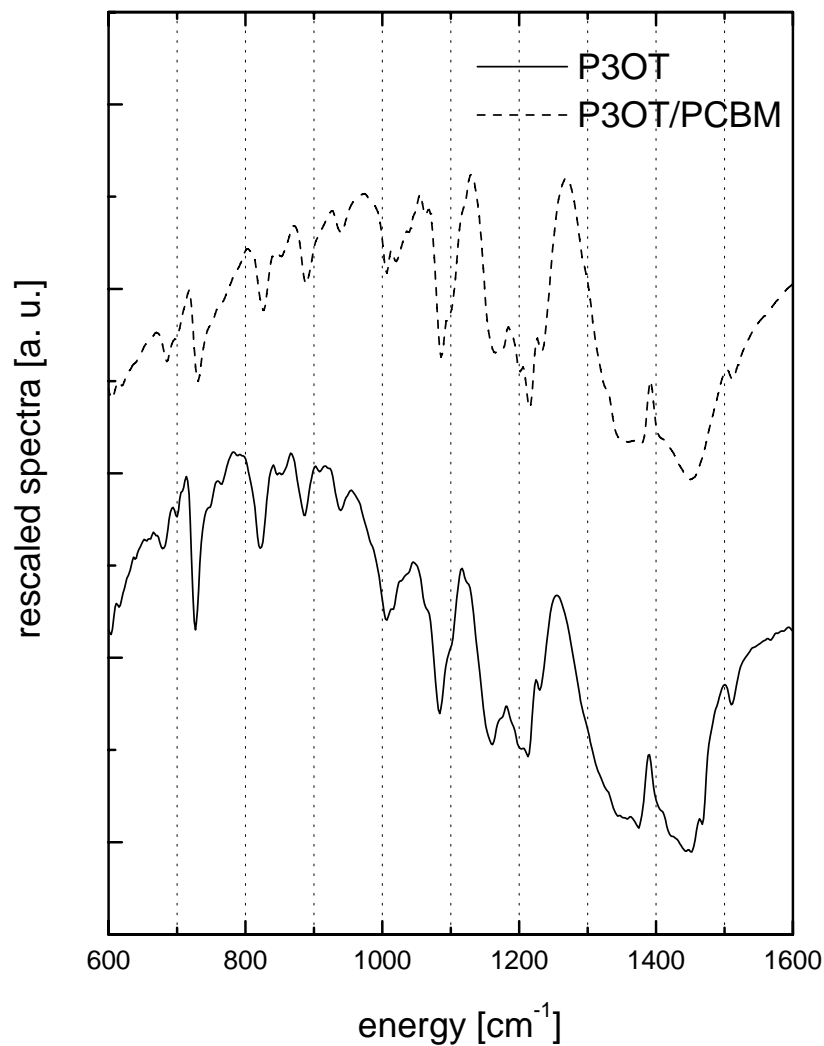


Figure 30: Enlarged low IR range for comparison of IRAV band positions for P3OT with and without PCBM.

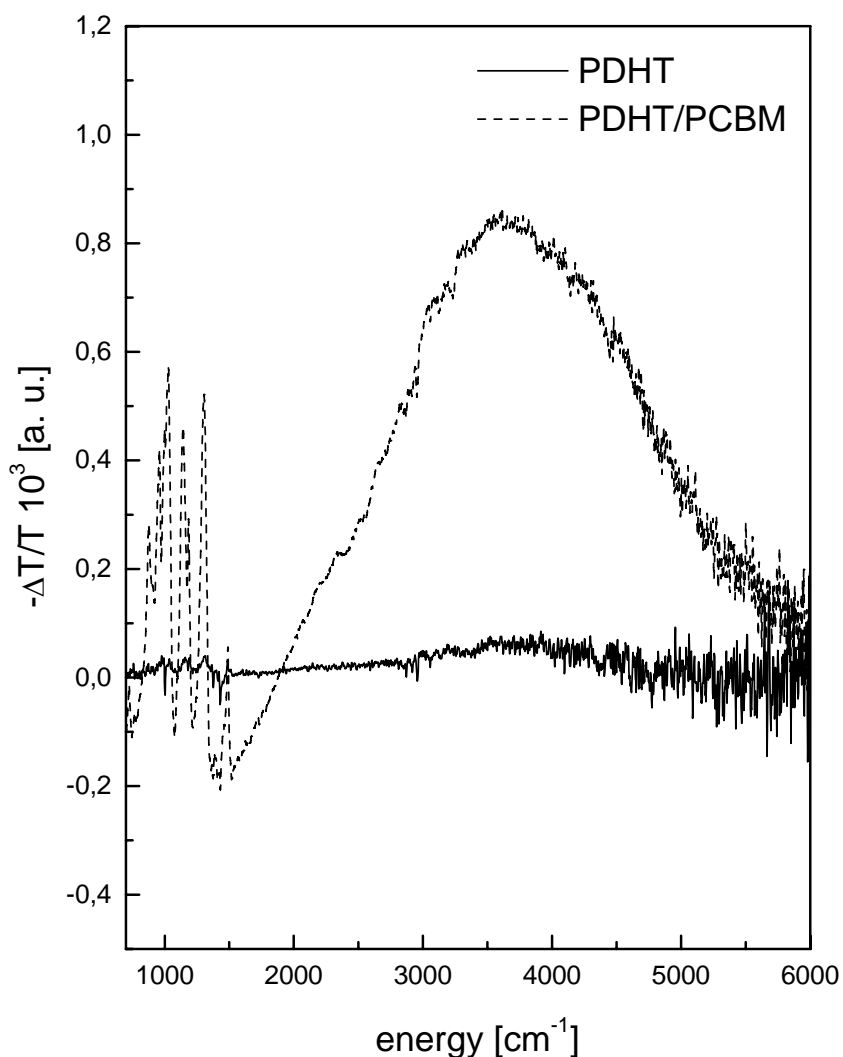


Figure 31: IR electronic absorption for PDHT with and without acceptor molecules within the network structure.

PDHT shows weaker photoinduced absorption both with and without presence of the acceptor molecules. Its polaron feature is much broader and the peak is at around 3700 cm^{-1} and FWHM exceeds 2000 cm^{-1} . The electronic transition absorption for P3OT is significantly lower in energy than most other conjugated polymers. This is important to mention and because of its shoulder feature one should at least consider the possibility that this peak in reality may consist of two absorption peaks close to each other.

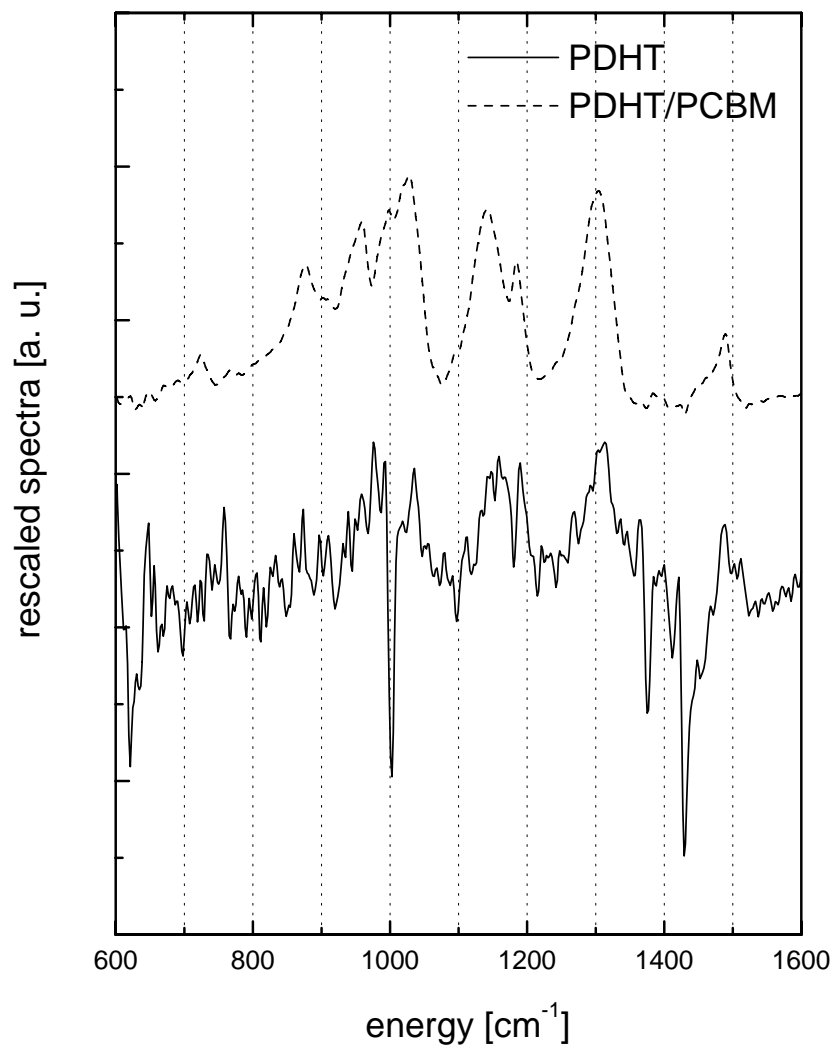


Figure 32: Enlarged low IR range for comparison of IRAV band positions for PDHT with and without PCBM.

6.3 Influence of host matrices

The photoactive materials can be protected by incorporation into other materials at which the charge transfer properties must maintain. Does the embedding of photoactive substances into a passive but stable conventional host polymer matrix influence the photophysical reactions between our active components? An investigation for the two conjugated polymers P3OT and PDHT follows.

6.3.1 Low energy range

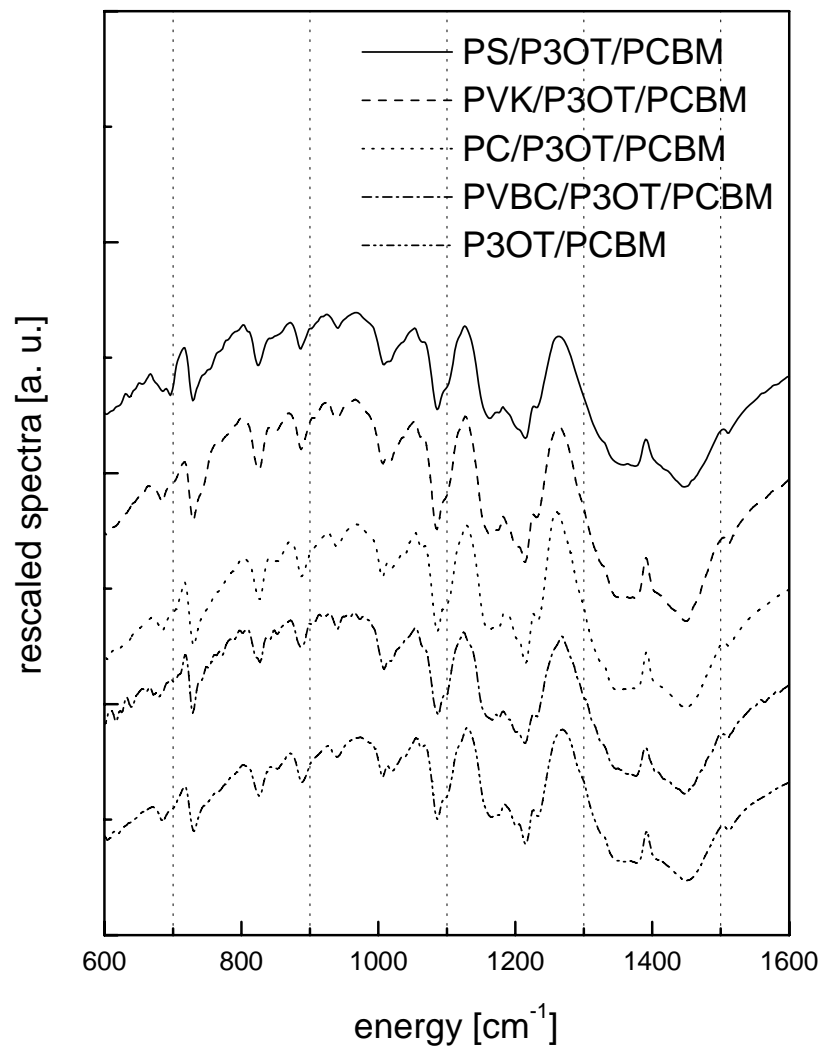


Figure 33: Host polymer influence on IRAV modes for P3OT.

We have incorporated the photoactive charge transfer systems P3OT/PCBM and PDHT/PCBM into different conventional polymers. There are differences in response depending on into which host polymer the photoactive is embedded, but in the low energy range ($< 2000 \text{ cm}^{-1}$) these only concern the strength of the photoinduced absorption and not the energetic positions of the absorption bands. These experiments are displayed in Figure 33 and Figure 34.

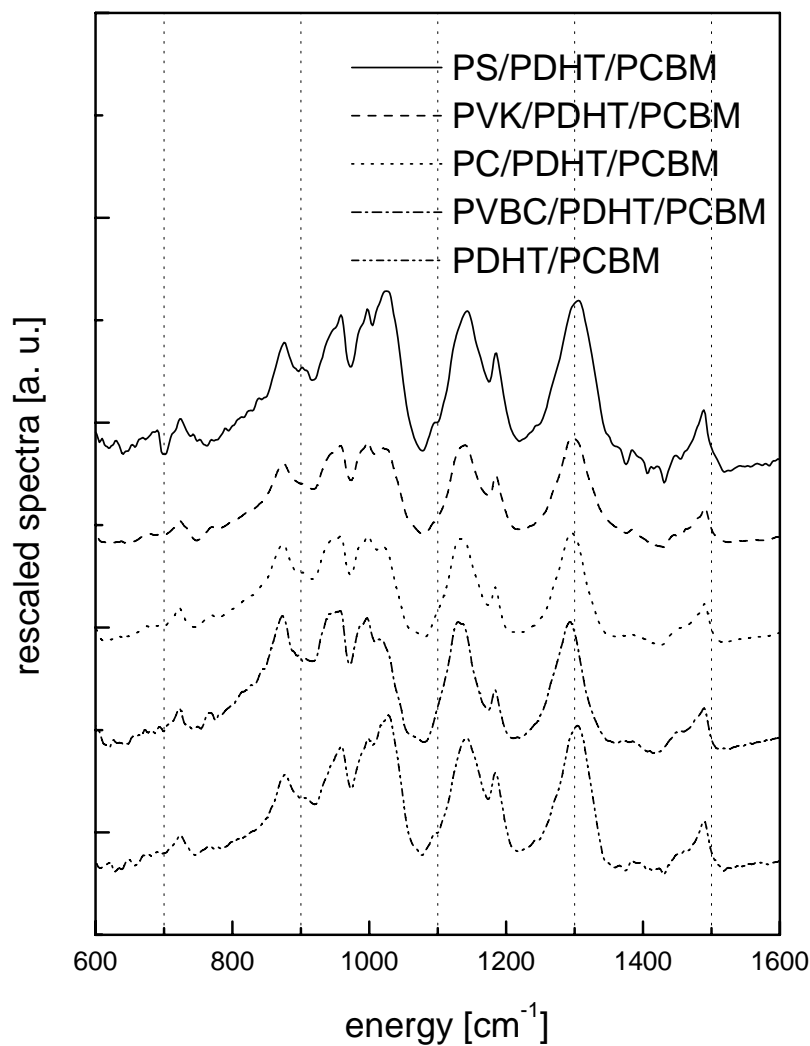


Figure 34: Host polymer influence on IRAV modes for PDHT.

Qualitatively we do not observe any changes regarding the shapes and positions of the IRAV modes or other influence by the conventional host polymer matrices in the low energy region. However, this is not the case for higher energies.

6.3.2 Higher energy range

Although each of the samples is diluted identically (1:1:1 and 1:1 respectively), we see that the absorption is suppressed differently for different hosts. The infrared absorption is weakened as expected because of dilution, which leads to less contact surface for the ultrafast electron transfer to take place at.

The polycarbonate host system shows unexpectedly strong infrared absorption and electron transfer, approximately the same magnitude as without host polymer when respect is taken to the lower concentration of active components. The reason for this behaviour probably it is due to insufficient blending giving rise to spots on the film with either only conjugated polymer or only polycarbonate.

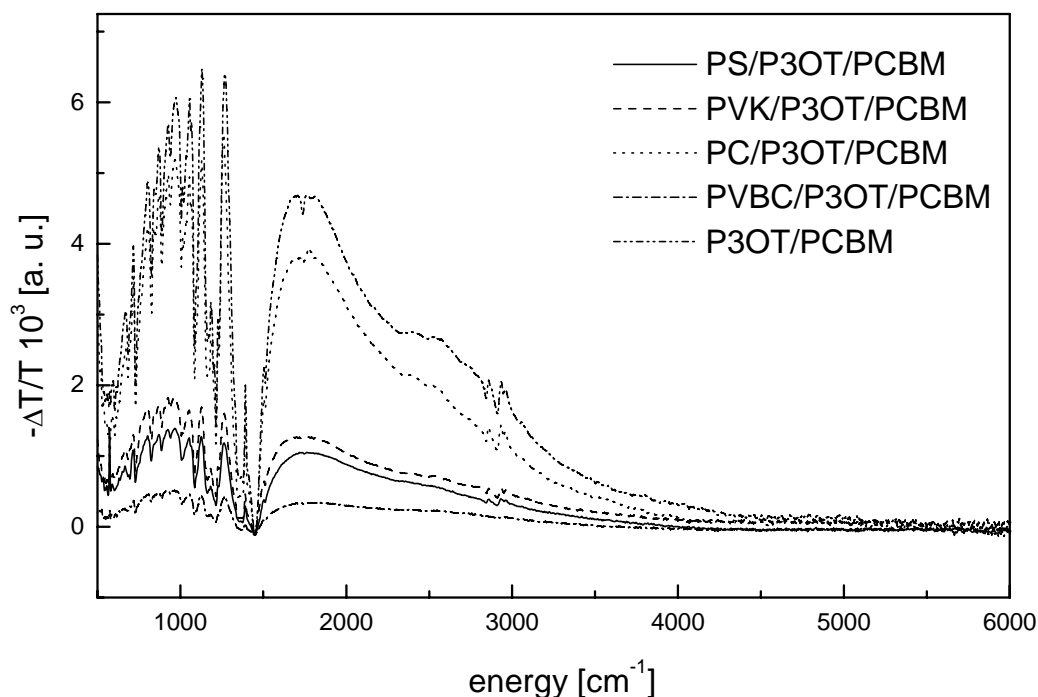


Figure 35: Weakening of photoinduced absorption for embedded P3OT/PCBM charge transfer network.

When we turn our attention to the embedded PDHT/PCBM donor-acceptor network we see a very different picture. The broader electronic transitions attributed to polaron peaks were recognised already but we see shifts of almost 1000 cm^{-1} . Especially the polycarbonate polaron feature is shifted far to lower energy.

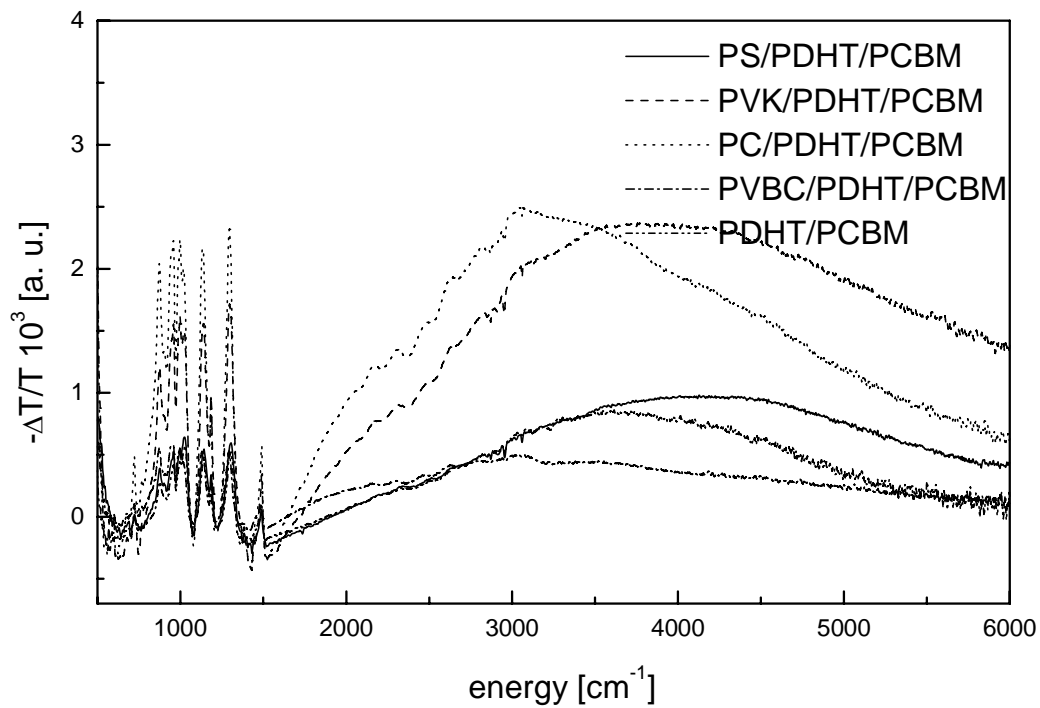


Figure 36: Photoinduced absorption for embedded PDHT/PCBM donor-acceptor networks.

We seem to have a heavily distorted system although the shifts do not appear in lower energy range. To determine the reasons for this surprising behaviour of the polycarbonate host, we take a look at the infrared absorption of the donor-acceptor network with and without the polycarbonate host. However, we observe the additional absorption in Figure 37 but there is no strong absorption in the 3000 cm^{-1} range exclusively for the polycarbonate host, which would explain this shift in the photoinduced absorption.

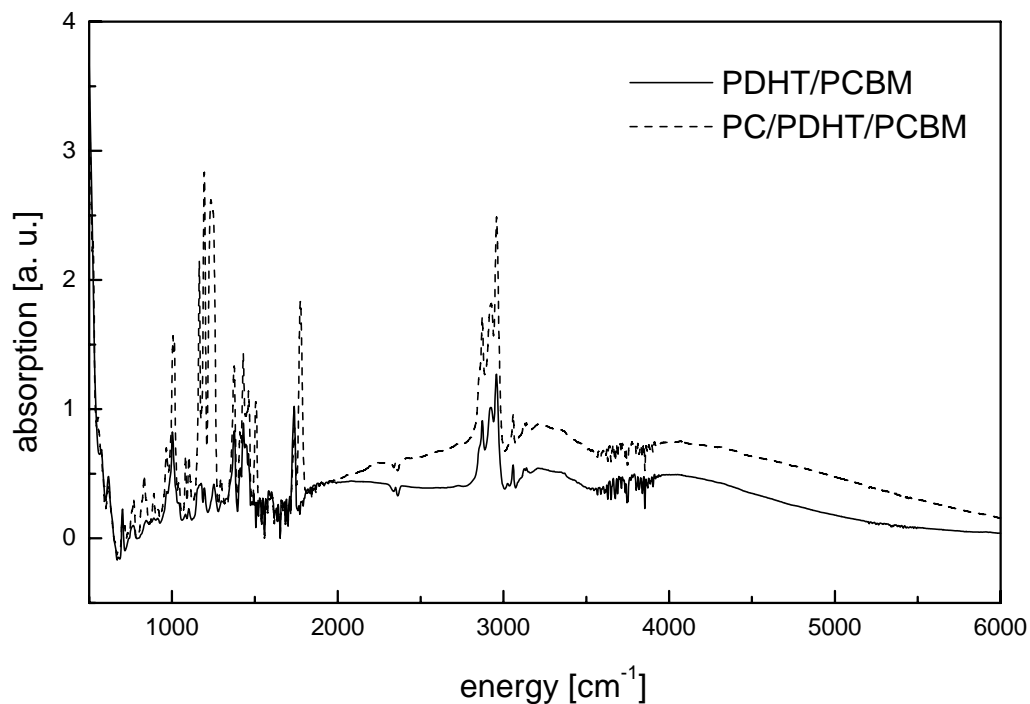


Figure 37: Absorption spectra for undoped PDHT/PCBM network with and without addition of PC host.

6.4 Morphology

Morphology is a parameter, which has to be taken into account very carefully when thinking about device production. A low ratio of fullerene is comparatively easy to add to the polymeric network structure. For photovoltaic devices that make use of percolation of fullerenes, a much higher acceptor concentration is necessary. In theory, hopping channels with one fullerene in contact with its neighbour fullerene, constituting electron transport channels through the interpenetrating network are created above 17 weight percent fullerene concentration. This is known as the percolation threshold concentration of 3-dimensional objects. In order to guarantee as good an electron transport as possible, the fullerene concentration must exceed the percolation threshold.

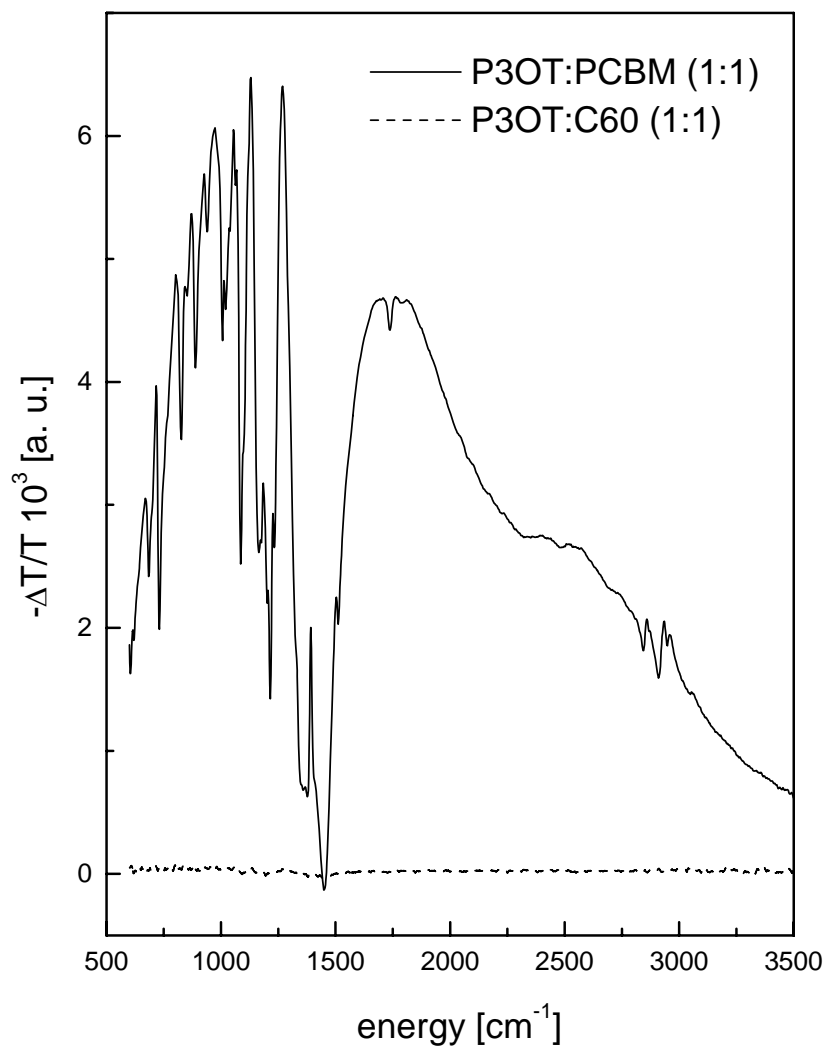


Figure 38: Improved morphology for PCBM derivative yields more charged species in the network.

For this reason the better soluble fullerene derivative PCBM is used instead of C₆₀. As can be seen in Figure 38, PCBM is more compatible, situates nearer to the donors and does not form clusters like C₆₀ does which leads to many more donor-acceptor interfaces and better conditions for the ultrafast photoinduced charge transfer to take place. There is a substantial enhancement of the photoinduced infrared absorption over the whole region. One peculiar observation is that lower concentration of C₆₀ (~5 weight percent) in the conjugated polymer/fullerene network seems to have higher IRAV intensity than a high concentration (~50 weight percent). We think that this is due to the differences in solubility for the network

constituents, which leads to a phase separation and hence a multilayer structure when one of the components stays longer than the other components in the evaporating solution.

We have seen unambiguous evidence for the electron transfer also from pure conventional polymer onto fullerene. As we see in the Figure 39 below there is a well defined but weak photoinduced absorption for PVK with a peak at 4700 cm^{-1} . This implies a possibility to use PVK as an additional donor in photoactive charge transfer heterojunctions. Pure PVK absorbs first at around 300 nm and the pump energy is only 488 nm . Most likely is a hole transfer from excited PCBM onto PVK, which enables this effect [36].

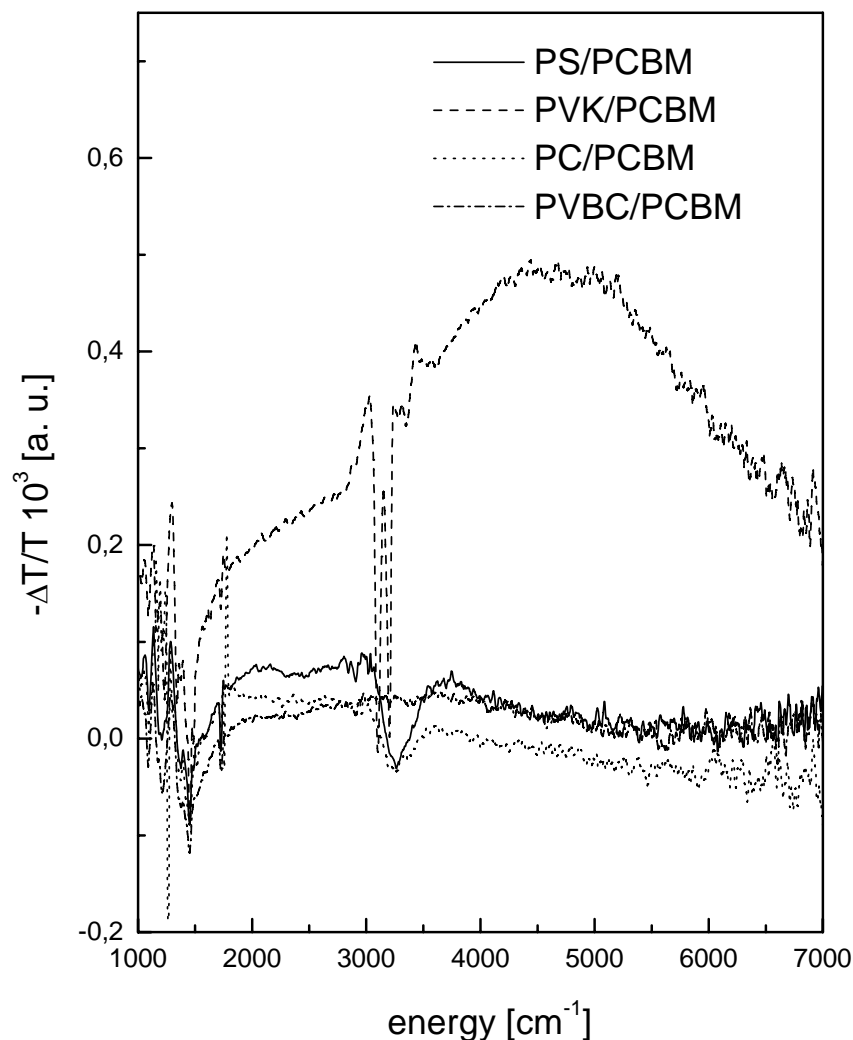


Figure 39: Evidence for electron donor functionality of the conventional polymer PVK (smoothed spectra).

6.5 Conclusions

- Comparison of different doping methods reveals conformity and correspondence of the IRAV bands. Especially for P3OT, we observe red shifted IRAV features for the photoinduced doping. These shifts can be described for polyacetylene with the amplitude mode (AM) theory. IRAV modes are shifted towards lower energies when the degree of chemical or electrochemical doping is increased.
- Addition of electron acceptors into the polymer matrix enhances the photoinduced infrared absorption by at least one order of magnitude, but does not change energetic positions neither for IRAV bands nor for other sub bandgap electronic absorption except for a vague shoulder-like feature for P3OT/PCBM (see Figure 29).
- P3OT/PCBM shows a stronger photoinduced infrared absorption than PDHT/PCBM and is therefore better suited as material in plastic solar cells.
- Embedding of the photoactive charge transfer system into a conventional polymer host matrix does not shift the positions of the lower range infrared bands. In the mid-infrared window we see shifts for PDHT but not for P3OT. Dilution of the heterojunction inhibits the ultrafast photoinduced charge transfer to different extent depending on the host polymer.
- The morphology of PCBM allows donors and acceptors in the network to interact more closely resulting in enhanced electron transfer performance compared to symmetric C₆₀.
- PVK, which is a conventional polymer, can be used as additional electron donor independent of conjugated polymers.

6.6 Acknowledgements

One year ago I was given opportunity and had the option to stay another year abroad and finish the diploma in Linz. It was no easy decision to make, but I am now convinced that I did right. The reasons for this are people in my immediate surrounding. I am indebted to many, Serdar for your enthusiasm, generosity and cut the crap advise, Christoph who has been a prerequisite for the whole work and Helmut, the most consistent man in middle Europe. I will remember each person at the institute for good co-operation and many laughs at tall but not necessarily true stories. Regina Bätje at CATT, who administrated the financial contribution which enabled the extended stay, Magnus Cedergren, who's major impact certificates helped

me through the jungle of bureaucracy, which sometimes seemed impenetrable, Olle for the hospitality at IFM in Linköping. Those of you who came visiting me meant a lot and of course everybody at home, in both countries, for supporting me throughout the whole work. Thanks!

7 Bibliography

- [1] S. Roth, *One-Dimensional Metals*, VCH, 1995.
- [2] F. Padinger, *Diploma Thesis*, Johannes Kepler University of Linz, 1998.
- [3] H. Neugebauer, C. J. Brabec, J. C. Hummelen, R. A. J. Janssen and N. S. Sariciftci, (in preparation).
- [4] C. J. Brabec, V. Dyakonov, N. S. Sariciftci, W. Graupner, G. Leising and J. C. Hummelen, *J. Chem. Phys.*, **109**, (in press).
- [5] Y. Wang and A. Suna, *J. Phys. Chem. B*, **101**, 5627, (1996).
- [6] P. M. Borsenberger and D. S. Weiss, *Organic Photoreceptors for Imaging Systems*, **153-272**, Marcel Dekker Inc., (1997).
- [7] U. W. Gedde, *Polymer physics*, Chapman & Hall, 1995.
- [8] C. K. Chiang, C. R. Fincher Jr., Y. W. Park, A. J. Heeger, H. Shirakawa, E. J. Louis, S. C. Gau and A. G. MacDiarmid, *Phys. Rev. Lett.*, **39**, 1098-1101, (1977).
- [9] N. C. Greenham, *PhD Thesis*, University of Cambridge, 1995.
- [10] R. E. Peierls, *Quantum Theory of Solids*, Oxford University Press, 1995.
- [11] P. W. Atkins, *Molecular Quantum Mechanics*, 2nd ed., Oxford University Press, 1982.
- [12] W. P. Su, J. R. Schrieffer and A. J. Heeger, *Phys. Rev. Lett.*, **42**, 1698-1701, (1979).
- [13] A. J. Heeger, S. Kivelson, J. R. Schrieffer and W.-P. Su, *Reviews of Modern Physics*, **60**, 781-850, (1988).
- [14] R. Pariser and R. G. Parr, *J. Chem. Phys.*, **21**, 767, (1953).
- [15] J. A. Pople, *Trans. Faraday Soc.*, **49**, 1375, 1953.
- [16] N. S. Sariciftci (ed.), *Primary Photoexcitations in Conjugated Polymers: Molecular Exciton vs. Semiconductor Band Model*, World Scientific Publishing Co. Pte. Ltd., 1997.
- [17] N. S. Sariciftci, L. Smilowitz, A. J. Heeger and F. Wudl, *Science*, **258**, 1474-1476, (1992).
- [18] B. Kraabel, D. McBranch, N. S. Sariciftci, D. Moses and A. J. Heeger, *Phys. Rev. B*, **50**, 18543-18552, (1994).
- [19] H. W. Kroto, J. R. Heath, S. C. O'Brien, R. F. Curl and R. E. Smalley, *Nature*, **318**, 162, (1985).
- [20] P. M. Allemand, A Koch, F. Wudl, Y. Rubin, F. Diederich, M. M. Alvarez, S. J. Anz and R. L. Whetten, *J. Am. Chem. Soc.*, **113**, 1050, (1991).
- [21] A. R. Kortan, N. Kopylov, S. H. Glarum, E. M. Gyorgy, A. P. Ramirez, R. M. Fleming, F. A. Thiel and R. C. Haddon, *Nature*, **355**, 529, (1992).
- [22] J. C. Hummelen, B. W. Wright, F. Lopez and F. Wudl, *J. Org. Chem.*, **60**, 532, (1995).
- [23] P. W. Atkins, *Physical Chemistry*, Oxford University Press, 1978.
- [24] H. Neugebauer, *Macromol. Symp.*, **94**, 61, (1995).

- [25] C. Petritsch, *Diploma Thesis*, Technische Universität Graz, 1996.
- [26] M Zagórska, A. Pron and S. Lefrant, *Handbook of Organic Conductive Molecules and Polymers*, vol. 3, **183-218**, H. S. Nalwa (ed.), John Wiley & Sons Ltd, 1997.
- [27] K. Lee, E. K. Miller, N. S. Sariciftci, J. C. Hummelen, F. Wudl and A. J Heeger, *Phys. Rev. B*, **54**, 10525-10529, (1996).
- [28] H. E. Schaffer and A. J. Heeger, *Solid State Comm.*, **59**, 415-421, (1986).
- [29] B. Horowitz, *Solid State Comm.*, **41**, 729-734, (1982).
- [30] E. Ehrenfreund, Z. V. Vardeny, O. Brafman and B. Horowitz, *Phys. Rev. B.*, **36**, 1535-1553, (1987).
- [31] A. Girlando, A. Painelli, G. W. Hayden and Z. G. Soos, *Chem. Phys.*, **184**, 139-148, (1994).
- [32] Z. G. Soos, A. Girlando and A. Painelli, *Mol. Cryst. Liq. Cryst.*, **256**, 711-719, (1994).
- [33] G. Zerbi, M. Gussoni and C. Castiglioni, *Conjugated Polymers*, **435-507**, J. L. Brédas and R. Silbey, (eds.), Kluwer Academic Publishers, (1991).
- [34] G. Zerbi, C. Castiglioni and M. Del Zoppo, *Electronic Materials: The Oligomer Approach*, **345-402**, K. Müllen and G. Wegner (eds.), Wiley-VCH, (1998).
- [35] K. Lee, R. A. J. Janssen, N. S. Sariciftci and A. J. Heeger, *Phys. Rev. B.*, **49**, 5781-5784, (1994).
- [36] Y. Wang, *Nature*, **356**, 585 (1992).

Other sources in alphabetical order, that have been used for this work:

- [37] C. N. Banwell and E. M. McCash, *Fundamentals of Molecular Spectroscopy*, 4th ed., McGraw-Hill International (UK) Limited, 1994.
- [38] C. Cuniberti, G. Dellepiane, P. Piaggio, R. Franco, G. F. Musso, C. Dell'Erba and G. Garbarino, *Chem. Mater.*, **8**, 708-713, (1996).
- [39] M. S. Dresselhaus, G. Dresselhaus and P. C. Eklund, *Science of Fullerenes and Carbon Nanotubes*, Academic Press, Inc., 1996.
- [40] E. Ehrenfreund and Z. V. Vardeny, *J. Inter. Soc. Opt. Engineering (SPIE)*, **3145**, 324-332, (1997).
- [41] Y. Furokawa, *J. Phys. Chem.*, **100**, 15644-15653, (1996).
- [42] A. Gilbert and J. Baggott, *Essentials of Molecular Photochemistry*, Blackwell Scientific Publications, 1991.
- [43] A. Girlando, A. Painelli and Z. G. Soos, *J. Chem. Phys.*, **98**, 7459-7465, (1993).
- [44] M. Granström, *PhD Thesis*, Linköping University, 1996.
- [45] W. Graupner, *PhD Thesis*, Technische Universität Graz, 1994.
- [46] P. R. Griffiths and J. A. de Haseth, *Fourier Transform Infrared Spectrometry*, John Wiley & Sons, Inc. 1986.

- [47] C. Hall, *Polymer Materials –an introduction for technologists and scientists*, The Macmillan Press Ltd., 1981.
- [48] L. B.-Å. Johansson, *Elements of Electronic Absorption and Emission Spectroscopy*, Umeå University, 1998.
- [49] H. G. Kiess (ed.), *Conjugated Conducting Polymers*, Springer-Verlag, 1992.
- [50] Y. H. Kim, S. Hotta and A. J. Heeger, *Phys. Rev. B.*, **36**, 7486-7490, (1987).
- [51] Y. H. Kim, S. Hotta and A. J. Heeger, *Phys. Rev. B.*, **38**, 5490-5495, (1988).
- [52] K. Lee, R. A. J. Janssen, N. S. Sariciftci and A. J. Heeger, *Mol. Cryst. Liq. Cryst.*, **256**, 739-744, (1994).
- [53] OPUS Spectroscopic Software, *Macro Programming Manual*, Bruker Analytische Meßtechnik GmbH, 1995.
- [54] J. Orenstein, *Handbook of Conducting Polymers*, vol. 2, chapt. 36, ed. T. Skotheim, Dekker/New York-Basel, 1986.
- [55] R. J. Van Overstraeten and R. P. Mertens, *Physics, Technology and Use of Photovoltaics*, Adam Hilger Ltd, 1986.
- [56] N. S. Sariciftci and A. J. Heeger, *Handbook of Organic Conductive Molecules and Polymers*, vol. 1, **413-455**, H. S. Nalwa (ed.), John Wiley & Sons Ltd, 1997.
- [57] R. M. Silverstein, G. C. Bassler and T. C. Morrill, *Spectrometric Identification of Organic Compounds*, 5th ed., John Wiley & Sons, Inc., 1991.
- [58] W. P. Su, J. R. Schrieffer and A. J. Heeger, *Phys. Rev. B*, **22**, 2099-2111, (1980).
- [59] M. Veronelli, M. C. Gallazzi and G. Zerbi, *Acta Polymer.*, **45**, 127-130, (1994).
- [60] M. Veronelli, M. C. Gallazzi and G. Zerbi, *Synthetic Metals*, **55-57**, 545-551, (1993).

8 Appendix

8.1 Specifications of used equipment

FT-IR spectrometer	Bruker IFS 66/S with OPUS 2.2 software.
UV-VIS spectrometer	Hitachi F-4010 with multi-sample holder.
Fluorescence spectrometer	Hitachi U-3210 with multi-sample holder.
Illumination source	Coherent Innova 400 argon ion laser with optical fibre transferring the beam.
Chopper system	Electromagnetic operation, software controlled switch.
Evacuation	Pfeiffer Duo pre-pump and Pfeiffer TSH 110 turbo-pump.

Table 3: Models, brands, performance and data of used equipment.

8.2 About this work

This work was carried out in the Institute for Physical Chemistry (IPC) at the Johannes Kepler University of Linz, Austria. It is a co-operation between IPC and the developing company Quantum Solar Energy Linz (QSEL) and was completed in September 1998 after a duration of twelve months. During the year I have attended scientific conferences and summer schools in Obdach (A), Kirchberg (A), Montpellier (F) and Hirschegg (D), where parts of this work were presented. All staff in IPC gave scientific guidance and supervision especially Dr. Christoph J. Brabec, Dr. Helmut Neugebauer and Prof. Dr. N. Serdar Sariciftci. Also thanks to Prof. Dr. Eitan Ehrenfreund for helpful discussions. Financial support was given by a European Commission grant, which was administrated by the Central Austrian Training in Technologies (CATT).

8.3 Publications

Parts of this work are to be published in scientific publications. Enclosed conference proceedings (ICSM 98, International Conference on Synthetic Metals) papers have been submitted.